Mathematical modeling of the Coronavirus (Covid-19) transmission dynamics using classical and fractional derivatives

Hamadjam Abboubakar[a,b,*], Reinhard Racke[b]

[a] *University of Ngaoundéré, University Institute of Technology, Department of Computer Engineering, LASE laboratory, P.O. Box 455, Ngaoundéré, Cameroon*
[b] *University of Konstanz, Department of Mathematics and Statistics, P.O. Box 78457 Konstanz, Germany*

Abstract

The goal of this work is the formulation and analysis of a Covid-19 transmission dynamics model which takes into account two doses of the vaccination process, confinement, and treatment with limited resources, using both integer and fractional derivatives in the Caputo sense. After the model formulation with classical derivative, we start by establishing the positivity, boundedness, existence, and uniqueness of solutions. Then, we compute the control reproduction number $\mathcal{R}_c$ and perform the local and global asymptotic stability of the disease-free equilibrium whenever $\mathcal{R}_c < 1$. We also prove the existence of at least one endemic equilibrium point whenever $\mathcal{R}_c > 1$. Using real data from Germany, we calibrate our models by performing parameter estimations. We find that the control reproduction number is approximately equal to 1.90, which shows that we are in an endemic state. We also perform global sensitivity analysis by computing partial rank correlation (PRCC) coefficients between $\mathcal{R}_c$ (respectively infected states) and each model parameter. After that, we formulate the corresponding fractional model in the Caputo sense, proving positivity, boundedness, existence, and uniqueness of solutions. We also compute the control reproduction number of the fractional model, which depends on the fractional order φ. We prove the local and global asymptotic stability of the disease-free equilibrium whenever the control reproduction number is less than one, as well as the existence of an endemic equilibrium point whenever the control reproduction number is greater than one. To validate our theoretical analysis of both models, and compare the two types of derivatives, we perform several numerical simulations. We find that for long-term forecasting, the fractional model, with a fractional order $\varphi \leq 0.87$ is better than the model with integer derivative.

Key words: COVID-19, Mathematical model, Control reproduction number, Asymptotic stability, Parameter estimation, Global sensitivity analysis, Caputo fractional derivative
2000 MSC: 34D20, 26A33, 47H10, 92D30,

(Version of November 3, 2022)

1. Introduction

COVID-19 is a disease caused by a new strain of coronavirus. The first case was reported in Wuhan, China in December 2019. Since then, the disease spread in many countries and

*Corresponding author
Email addresses: h.abboubakar@gmail.com & hamadjam.abboubakar@uni-konstanz.de (Hamadjam Abboubakar[a,b,*]), reinhard.racke@uni-konstanz.de (Reinhard Racke[b])

became a pandemic [61]. The virus called the SARS-CoV-2 virus spreads generally population through close contact with an infected person or with an infected object. According to currently available data, the virus is mainly spread by respiratory droplets between people who are in close contact with each other [23].

At the beginning of the pandemic, the absence of a general Covid-19 pre-existing immunity in humans as well as the absence of curative drugs and vaccines, have guided the choice of several countries to implement non-pharmaceutical interventions that include social distancing, hand-washing, confinement, isolation which is recommended in order to stop the spread of the virus [43]. As of May 2021, different COVID-19 vaccines were authorized in some countries. For emergency or full use, seventeen vaccines have been approved by at least one stringent regulatory authority recognized by the World Health Organization (WHO) [62].Twenty five (26) other vaccines are in the test phase [62].

The problem remains the efficiency of each proposed vaccine [35, 60]. A mini-review discussing the reliability and efficiency of Covid-19 Vaccines revealed that four of the available vaccine had an efficacy greater than 80% (Pfizer-BioNTech ($\approx$ 95%), Moderna ($\approx$ 94%), Sputnik V ($\approx$ 92%), and Oxford-AstraZeneca ($\approx$ 81%)) [12]. However, it has been found that Covid-19 vaccines permit the alleviation of severe adverse reactions to the disease. This is why there has been a real reduction in the number of hospitalizations as well as deaths linked to Covid-19 in countries in which the level of vaccination coverage is high [5, 12].

Since the work of Sir Ronald Ross on malaria [46], mathematical modeling is used to describe transmission mechanisms as well as estimation and choice of control strategies. One of the first mathematical models, which was formulated to describe the new coronavirus transmission dynamics, is the model proposed in [32] by Zhihua his collaborators. The authors developed a Susceptible-Infectious-Symptomaric reported cases-Unreported cases-Removed epidemiological model to predict the Covid-19 epidemic in Wuhan. Chen et *al.* [4] also developed a Bats-Hosts-Reservoir-People transmission network model for simulating the potential transmission from the infection source (probably bats) to the human infection. They estimated the value of the basic reproduction number $\mathcal{R}_0$ of 3.58 (in fact, infection between reservoir and human gives a basic reproduction number equal to 2.30, and 3.58 from human to human). They conclude that the transmissibility of SARS-CoV-2 is higher than the Middle East respiratory syndrome (MERS) in the Middle East countries. Taking into account the existence of the super-spreader of the coronavirus, Ndaïrou et *al.* [42] formulate a compartmental model for the spread of the Covid-19 disease with application to Wuhan reported cases. Since then, several other model were also developed [2, 11, 13, 26, 27, 28, 40, 43]. Several works are conducted to evaluate the impact of vaccination on the fight against Covid-19 spread [30, 38, 37, 44, 47, 54]. In [44], the authors formulate a compartmental model to examine the impact of the use of three vaccine-types (Pfizer, Moderna and Janssen) on the on the dynamics of COVID-19 in a population. They use available data for these three vaccine-types to calibrate their model. They concluded through numerical simulations that the three vaccine-types permit to decrease the total number of individuals with severe Covid-19 illness, this means hospitalized persons. Moore et *al.* in [38, 37] used a mathematical model structured by age and UK region to evaluated the use of Covid-19 vaccine as only control strategy. The obtained results permitted to conclude that vaccination alone is insufficient to contain the outbreak. In the same way, Watson et *al.* [59] concluded that vaccination has permitted to prevent 14.4 million deaths, due to the Coronavirus, in 185 countries and territories between Dec 8, 2020, and Dec 8, 2021.

To estimate the costs of hospitalization, vaccination and the economic benefits of the

reducing Covid-19 deaths, Du et *al.* in [13] developed a multi-scale model which takes into account population-level transmission and individual-level vaccination. Their model consists of ten compartments in which two compartments stand for the two vaccine doses. They did not consider the environmental infection by indirect contact with tools infected by a infectious persons. To assess age-specific vaccine allocation strategies in India, Foy and coworkers in [16] used an age-structured, expanded SEIR model with social contact matrices. Through numerical simulations, they concluded that depending on vaccine characteristics, people belonging to older age groups must be a priority in vaccine allocation. A statistical model in which social and SARS-CoV-2 epidemiological dynamics interact with one another is developed by Jentsch and coworkers [25]. The following vaccination strategies were taken into account: oldest-first strategy (those aged 60 years and older), youngest-first strategy (those younger than 20 years), uniform strategy (vaccinating uniformly by age), and a novel contact-based strategy. They concluded that the choice of the most effective vaccination strategy depends on the time course of the disease in the population, and for later vaccination campaigns, Covid-19 vaccines to interrupt transmission might prevent more deaths than prioritizing vulnerable age groups. In [49], Shen et *al.* formulated and studied a compartmental Covid-19 model in which vaccination is combined with the prevention, the rapid screening of exposed individuals, and infected individuals without screening. Through optimal control tools, they concluded that combined control measures can be used to minimize the disease burden. However, their model only considers a unique vaccine dose.

It should be noted that most of the Covid-19 models existing in the literature are either formulated using classical derivatives (integer derivatives) [11, 34, 42, 43] or using fractional derivatives (Caputo, Caputo-Fabrizio, Atangana-Baleanu,...) [27, 28, 31, 40, 41, 56, 50]. The latter are increasingly used in the modeling of infectious diseases. The given reason is that they have the great advantage of having a memory effect, compared to classical derivatives [6, 24, 58, 64]. The memory effect in the Covid-19 pandemic was emphasized by Sofonea et *al.* in [52]. Fractional derivatives give flexibility to decision-makers. Indeed, choosing the optimal value of fractional order, one can decide the start and the end date of the control measure strategies [40].

In the present work, we formulate and analyze an SEIR extended model in which we take into account quarantine, two vaccine doses, and the treatment of symptomatic persons in the presence of limited resources. We use both integer and non-integer derivatives. The goal here is to know which of the two types of derivatives can be used to better forecast the Covid-19 pandemic in Germany, and which fractional order better fit the reported case data. After the model formulation with integer derivatives, we prove the positivity, boundedness, existence, and uniqueness of solutions. We then compute the control reproduction number denoted by $\mathcal{R}_c$ and prove the local as well as global stability of the Covid-19 free equilibrium point whenever $\mathcal{R}_c < 1$. We also prove the existence of at least one endemic equilibrium point and give the condition of its local stability when $\mathcal{R}_c > 1$. Using the daily infected reported cases in Germany from February 15, 2021, to April 05, 2021, we calibrate the model by performing parameter estimation. By fixing the vaccine coverage at 70%, the vaccine efficacy on the disease dynamics is depicted through numerical simulations. We then perform global sensitivity analysis by computing the partial rank correlation coefficients between $\mathcal{R}_c$ (respectively infected states) and each model parameters. In the second part of the work, we present the corresponding fractional model in the Caputo sense and prove the positivity, boundedness, existence, and uniqueness of solutions of the fractional model. We compute the corresponding control reproduction which depends on the fractional order φ.

Indeed when $\varphi = 1$, the two models have the same threshold which governs their dynamics. We also prove the local stability of the disease-free equilibrium for the fractional model and deduce from the existence of the endemic equilibrium point of the integer model, the existence of at least one endemic equilibrium of the fractional model too. We then present the numerical scheme used to simulate the fractional model. We perform several numerical simulations to validate our analytical results and to compare the use of classical derivatives with fractional derivatives in the Caputo sense by determining which model better fit the German data, in a long-term dynamics.

The present work is structured as follows: Section 2.1 is devoted to the model formulation with classical derivative (Ordinary differential equations) and its mathematical analysis. Section 3 is devoted to model calibration and global sensitivity analysis. The formulation and analysis of the fractional model are done in Section 4. Numerical simulations of both models are done in Section 5. A conclusion and perspectives round up the work.

2. The ODE model

2.1. Model formulation

Before formulating our model, it is important to fix some hypotheses:

$\mathcal{H}_1$: There are no infected immigrants;

$\mathcal{H}_2$: Only non-infectious persons are vaccinated and recovered persons do not get the vaccine;

$\mathcal{H}_3$: Persons who are hospitalized (in situations of respiratory assistance) do not participate to the disease spread;

We denote the human population at any time by $N(t)$. Depending on their epidemiological status, we split the total human population into nine sub-classes called compartments. Thus, compartment S denotes susceptible individuals, Q is for quarantined individuals, V_1 is for susceptible individuals who have received the first vaccine dose against Covid-19, while V_2 is for individuals in V_1 state who have received the second vaccine dose against Covid-19. Since the infected individuals will become infectious after a period of 2 to 14 days, we consider the latent compartment E. After this stage, a fraction of infected individuals will become asymptomatic infected and enter the compartment denoted by A, and the other fraction will become symptomatic infected and will enter the compartment I. Among asymptomatic individuals, some of them will be recovered and become partially immunized (denoted by R, and a few of them will enter the compartment of individuals who need respiratory assistance and/or other specific treatments (denoted by H). A fraction of symptomatic individuals will become recovered (R), and another fraction can need specific treatments and/or respiratory assistance, and so will enter the compartment of hospitalized individuals denoted by H. In this model, we take into account the partial immunity of recovered individuals. Thus, after recovering from the disease, some people can become infected again. Contrary to Atifa et *al.* [2], we assume that recovered individuals do not enter the infectious compartments directly. Indeed, we assume that they must observe the necessary 2 days to become infected again. Contrary to several models in the existing literature (see [40, 43] and some references therein), we consider the fact that an uninfected person can become infected through a contact, for example, with the door handles, and the fact to eat or drink from the same dish or cup used by an infected person without disinfecting it. To model this phenomenon, we include the compartment B which stands for the density of free viruses in nature [11].

It is important to note that the vaccines available against Covid-19 do not confer perfect immunity against this disease. Thus, we include this in our model by the fact that vaccinated individuals can be infected regardless of their vaccination status (V_1 or V_2).

Dynamics of S. Susceptible individuals increase with the rate $r_2\Lambda$, where Λ denotes the recruitment rate and r_2 is the proportion of newcomers who enter the susceptible compartment. They decrease either by quarantine at a rate c_2, or by natural death at a rate μ, or by vaccination at a rate v_1, or by contact with an infected person or a material used by an infected person at a rate λ given by

$$\lambda(t) := \beta_1 \frac{A(t) + I(t)}{N(t) - H(t)} + \beta_2 \frac{\mathcal{B}(t)}{K + \mathcal{B}(t)}. \tag{1}$$

In Eq. (1), β_1 is the transmission probability from a infectious individual (either asymptomatic A or symptomatic I) to a uninfected individual (S, Q, V_1, and V_2); β_2 is the exposure rate to the free viruses in the environment; The half-saturation constant parameter denoted by K represents the concentration of free virus that yields 50% of chance for a susceptible individual to catch the coronavirus [11].

$$\frac{dS}{dt} = r_2\Lambda + c_1 Q(t) - \left[\overbrace{v_1 + \mu + c_2}^{k_1} + \phi_2 \overbrace{\left(\beta_1 \frac{A(t) + I(t)}{N(t) - H(t)} + \beta_2 \frac{\mathcal{B}(t)}{K + \mathcal{B}(t)} \right)}^{\lambda(t)} \right] S(t). \tag{2}$$

Dynamics of Q. The compartment of quarantined persons increases with either the rate $r_1\Lambda$, where Λ denotes the recruitment rate and r_1 is the proportion of new quarantined persons who enter the system, or with a rate c_1 of susceptible persons who are quarantined due to their exposure or contact with an infected individual. They decrease either by natural mortality rate μ, by end of quarantined by returning in the compartment of susceptible individuals with a rate c_1, or or by contact with an infected person or a material used by an infected person at a rate λ described by Eq. (1).

$$\frac{dQ}{dt}(t) = r_1\Lambda + c_2 S(t) - \left(\overbrace{\mu + c_1}^{k_2} + \phi_1 \lambda(t) \right) Q(t). \tag{3}$$

Dynamics of V_1. The compartment of vaccinated persons who have taken the first dose increases with either the rate $r_3\Lambda$, where Λ denotes the recruitment rate and r_3 is the proportion of vaccinated persons with the first dose who enter the system or with the susceptible individuals who have taken for the first time the Covid-19 vaccine at the rate v_1. They decrease either by natural mortality rate μ, by taking the second dose of vaccine at a rate v_2, or by contact with an infected person or a material used by an infected person at a rate λ described by Eq. (1).

$$\frac{dV_1}{dt}(t) = r_3\Lambda + v_1 S(t) - \left(\overbrace{\mu + v_2}^{k_3} + \phi_3 \lambda(t) \right) V_1(t). \tag{4}$$

Dynamics of V_2. The compartment of vaccinated persons who have taken the second dose increases with either the rate $(1-r_1-r_2-r_3)\Lambda$, or with the vaccinated individuals who have taken the first dose of the Covid-19 vaccine at the rate v_2. They decrease either by natural mortality rate μ, or by contact with an infected person or a material used by an infected person at a rate λ described by Eq. (1).

$$\frac{dV_2}{dt}(t) = \overbrace{(1-r_1-r_2-r_3)}^{\pi_1}\Lambda + v_2V_1(t) - (\mu+\phi_4\lambda(t))\,V_2(t). \tag{5}$$

Dynamics of E. Exposed persons are uninfected individuals (S, Q, V_1, V_2, and R) who have contracted the Coronavirus (Covid-19) but are not yet infectious. Their number increases with the flow due to susceptible individuals S, quarantined individuals Q, vaccinated individuals for the first time V_1, vaccinated individuals with the second dose V_2 and recovered individuals R, who have had close contact with infected individuals (A or I). They decrease by natural mortality with a rate μ, or by becoming either asymptomatic (A) with a rate $(1-q)\gamma$ or symptomatic (I) with a rate $q\gamma$, where $\dfrac{1}{\gamma}$ is the average incubation period, and q is a proportion of exposed person who will become symptomatic.

$$\frac{dE}{dt}(t) := \lambda(t)\,(\phi_5R(t)+\phi_1Q(t)+\phi_2S(t)+\phi_3V_1(t)+\phi_4V_2(t)) - \overbrace{(\mu+\gamma)}^{k_4}E(t). \tag{6}$$

Dynamics of A. The compartment of asymptomatic persons increases with a flow $(1-q)\gamma$ of exposed persons and decreases either by natural mortality at a rate μ, by becoming either hospitalized at a rate $\psi_2\theta$, recovered at a rate $\psi_1\theta$, or by becoming symptomatic at a rate $(1-\psi_1-\psi_2)\theta$, where θ stand for the transition rate to remainder states (I, H, R).

$$\frac{dA}{dt}(t) := \overbrace{(1-q)}^{p}\gamma E(t) - \overbrace{(\mu+\theta)}^{k_5}A(t). \tag{7}$$

Dynamics of I. The compartment of symptomatic persons increases with a flow $q\gamma$ of exposed persons to which we add a flow of $(1-\psi_1-\psi_2)\theta$ of asymptomatic persons; It decreases either by natural mortality at a rate μ increased by the disease-induced death rate δ_1, by becoming either hospitalized at a rate $(1-\eta)\nu$, or recovered at a rate $\eta\nu$, where ν stand for the transition rate to hospitalized compartment and recovered compartment.

$$\frac{dI}{dt}(t) := q\gamma E(t) + \overbrace{(1-\psi_1-\psi_2)}^{\pi_2}\theta A(t) - \overbrace{(\mu+\delta_1+\nu)}^{k_6}I(t). \tag{8}$$

Dynamics of H. The compartment of hospitalized persons includes $\psi_2\theta$ of asymptomatic persons to which we add a rate $(1-\eta)\nu$ of symptomatic individuals. It decreases either by natural mortality at a rate μ increased by the disease mortality rate δ_2, or by healing with a healing rate ζ, or by specific health care that is impacted by the limited medical resources (for hospitalized persons requiring respiratory assistance) described as in [48, 65] by function

$$T(\sigma, H(t))(t) = \frac{\sigma H(t)}{\Phi + H(t)}, \tag{9}$$

with the parameter σ representing the medical resources supplied per unit time and Φ corresponds to half-saturation constant. Thus, the dynamics of H is given by

$$\frac{dH}{dt}(t) := \psi_2\theta A(t) + \overbrace{(1-\eta)}^{\pi_3}\nu I(t) - \overbrace{(\mu+\delta_2+\zeta)}^{k_7}H(t) - T(\sigma, H(t)). \tag{10}$$

Dynamics of R. The compartment of recovered individuals includes $\psi_1\theta$ rate of asymptomatic persons, $\eta\nu$ rate of symptomatic persons and $\zeta + T(\sigma, H)$ rate of hospitalized persons. It decrease either by natural mortality at a rate μ, or by infection by a rate λ described by Eq. (1).

$$\frac{dR}{dt}(t) := \psi_1\theta A(t) + \nu\eta I(t) + \zeta H(t) + T(\sigma, H(t))(t) - (\mu + \phi_5\lambda(t))\, R(t). \tag{11}$$

Dynamics of $\mathcal{B}$. Infectious individuals when they sneeze or cough without protection spill small droplets that contain thousands of viruses that will spread through the air, thus directly or indirectly infecting healthy people. We assume that only asymptomatic and symptomatic individuals contribute to the virus spread in the environment, with a rate of α_1 and α_2, respectively. The mortality rate of Coronavirus is denoted by τ.

$$\frac{d\mathcal{B}}{dt}(t) := \alpha_1 A(t) + \alpha_2 I(t) - \tau\mathcal{B}(t). \tag{12}$$

Putting Eqs.(2)–(12) together gives the following system expressed using ordinary derivatives:

$$\begin{cases} \frac{dS}{dt}(t) &= r_2\Lambda + c_1 Q(t) - (k_1 + \phi_2\lambda(t))\, S(t), \\ \frac{dQ}{dt}(t) &= r_1\Lambda + c_2 S(t) - (k_2 + \phi_1\lambda(t))\, Q(t), \\ \frac{dV_1}{dt}(t) &= r_3\Lambda + v_1 S(t) - (k_3 + \phi_3\lambda(t))\, V_1(t), \\ \frac{dV_2}{dt}(t) &= \pi_1\Lambda + v_2 V_1(t) - (\mu + \phi_4\lambda(t))\, V_2(t), \\ \frac{dE}{dt}(t) &= \lambda(t)\,(\phi_5 R(t) + \phi_1 Q(t) + \phi_2 S(t) + \phi_3 V_1(t) + \phi_4 V_2(t)) - k_4 E(t), \\ \frac{dA}{dt}(t) &= p\gamma E(t) - k_5 A(t), \\ \frac{dI}{dt}(t) &= q\gamma E(t) + \pi_2\theta A(t) - k_6 I(t), \\ \frac{dH}{dt}(t) &= \pi_3\nu I(t) + \psi_2\theta A(t) - k_7 H(t) - T(\sigma, H(t)), \\ \frac{dR}{dt}(t) &= \zeta H(t) + T(\sigma, H(t))(t) + \nu\eta I(t) + \psi_1\theta A(t) - (\mu + \phi_5\lambda(t))\, R(t), \\ \frac{d\mathcal{B}}{dt}(t) &= \alpha_1 A(t) + \alpha_2 I(t) - \tau\mathcal{B}(t). \end{cases} \tag{13}$$

We set $x = (S, Q, V_1, V_2, E, A, I, H, R, B)'$ the vector of state variables and

$$\mathbb{R}^{10}_+ = \left\{ x \in \mathbb{R}^{10} : x_i \geq \mathbf{0}, i \in [1; 10] \cap \mathbb{N} \right\}.$$

System (13) can rewritten in the following compact form

$$\begin{cases} \frac{dx}{dt} = \mathcal{F}(t, x) = (\mathcal{F}_1(x), \mathcal{F}_2(x), ..., \mathcal{F}_{10}(x))', \\ x(t_0) = x_0 = (S_0, Q_0, V_{10}, V_{20}, E_0, A_0, I_0, H_0, R_0, B_0)' \in \mathbb{R}^{10}_+, \end{cases} \tag{14}$$

where $\mathcal{F} : \mathbb{R}^{10} \to \mathbb{R}^{10}$ represents the right hand-side of (13), and $(\bullet)'$ stands for the transposition operator.

Table 1: Description of model parameters.

Parameter	Description
Λ	Recruitment rate
μ	Natural mortality rate
β_1	Direct contact rate
β_2	Indirect contact rate
r_1	Proportion of newcomers to the Q compartment
r_2	Proportion of newcomers to the S compartment
r_3	Proportion of newcomers to the V_1 compartment
v_1	First dose vaccination rate
v_2	Second dose vaccination rate
c_1	The rate of flow between Q to S
c_2	The rate of flow between S to Q
γ	Incubation period
q	Proportion of people in the E-compartment who will become asymptomatic
θ	The rate of flow between A to I, H, R-compartments
ψ_1	Proportion of people in the A-compartment who will recover from the disease
ψ_2	Proportion of people in the A-compartment who will become Hospitalized
ν	The rate of flow between I to H, R-compartments
η	Proportion of people in the I-compartment who will recover from the disease
δ_1	Disease-induced death for symptomatic people
δ_2	Disease-induced death for hospitalized people
ζ	Recovered rate of Hospitalized people
σ	Medical resources supplied per unit time
Φ	Half-saturation constant
α_1	Rate of virus spread to the environment by asymptomatic people
α_2	Rate of virus spread to the environment by symptomatic people
τ	The natural death rate of coronavirus in the environment
K	Half-saturation constant
ϕ_i, $i \in [1;5] \cap \mathbb{N}$	Modification parameters

Remark 1. *Hospitalized people (H) are not included in the force of infection. Indeed, we assume that people in respiratory assistance (hospitalized individuals) due to the infection to the coronavirus are not taking part in the active population who contribute to the transmission dynamics of the disease [43].*

2.2. Mathematical analysis

2.2.1. Positivity and Boundedness of solutions

We have the following result

Theorem 1. *(Positivity) Each solution* $x(t) = (S(t), Q(t), V_1(t), V_2(t), E(t), A(t), I(t), H(t), R(t), \mathcal{B}(t))^t$ *of model (13) with non-negative initial conditions* $x(0) = (S(0), Q(0), V_1(0), V_2(0), E(0), A(0), I(0), H(0), R(0), \mathcal{B}(0))^t \in \mathbb{R}^{10}_+$ *is non-negative for all* $t > 0$.

Proof. See Appendix A. □

Before proving the boundedness of solutions of systems (13), let us define the following subset of $\mathbb{R}^{10}_+$

$$\Upsilon = \left\{ x = (S, Q, V_1, V_2, E, A, I, H, R, \mathcal{B})' \in \mathbb{R}^{10}_+ : \left(\sum_{i=1}^{9} x_i \right) \leq \frac{\Lambda}{\mu}, \;\; x_{10} \leq \frac{(\alpha_1 + \alpha_2)\Lambda}{\mu\tau} \right\}. \tag{15}$$

The following result holds.

Theorem 2. *(Boundedness of solutions) The region Υ is positively invariant and attracting for system (13).*

Proof. See Appendix B. □

2.2.2. Existence and uniqueness of solutions

Before proving the existence and uniqueness, let us claim the following result.

Lemma 1. *The function $\mathcal{F} : \mathbb{R}^{10} \to \mathbb{R}^{10}$ defined in (14) is a continuously differentiable function on $\mathbb{R}^{10}$.*

Proof. See Appendix C.

□

From Lemma 1, the following result holds.

Lemma 2. *The continuously differentiable function $\mathcal{F} : \mathbb{R}^{10} \to \mathbb{R}^{10}$ defined in (14) is locally Lipschitz continuous on $\mathbb{R}^{10}$.*

Theorem 3 (Existence-uniqueness)**.** *With Theorem 2, and for initial conditions $x_0 = (S_0, Q_0, V_{10}, V_{20}, E_0, A_0, I_0, H_0, R_0, \mathcal{B}_0)' \in \mathbb{R}^{10}_+$, the Covid-19 transmission model (13) admits a unique solution $x \in \mathcal{C}([0; +\infty[, \mathbb{R}^{10}_+)$.*

2.2.3. The control reproduction number

First of all, it is important to note that in the absence of disease, that is $E = A = I = H = \mathcal{B} = 0$, system (13) admits always one stationary point, also called disease-free equilibrium (DFE), $\mathcal{E}_0 = (S_0, Q_0, V_{10}, V_{20}, 0, 0, 0, 0, 0, 0)'$ where

$$\begin{cases} S_0 &= \dfrac{[c_1 (c_2 r_2 + k_1 r_1) + (k_1 k_2 - c_1 c_2) r_2] \Lambda}{k_1 (k_1 k_2 - c_1 c_2)}, \\ Q_0 &= \dfrac{(c_2 r_2 + k_1 r_1) \Lambda}{k_1 k_2 - c_1 c_2}, \\ V_{10} &= \dfrac{[(k_1 k_2 - c_1 c_2) r_3 + v_1 (k_2 r_2 + c_1 r_1)] \Lambda}{(k_1 k_2 - c_1 c_2) k_3}, \\ V_{20} &= \dfrac{[(k_1 k_2 - c_1 c_2) (v_2 r_3 + \pi_1 k_3) + (k_2 r_2 + c_1 r_1) v_1 v_2] \Lambda}{(k_1 k_2 - c_1 c_2) k_3 \mu}. \end{cases} \tag{16}$$

with $k_1 k_2 - c_1 c_2 = \mu^2 + (c_2 + v_1 + c_1)\mu + c_1 v_1 > 0$. From (16), we have $N_0 := S_0 + Q_0 + V_{10} + V_{20} = \dfrac{\Lambda}{\mu}$.

To compute the control reproduction number, denoted by $\mathcal{R}_c$, we will use the next generation approach (see [7, 57]). Let us set $y = (E, A, I, H, \mathcal{B})'$. The vector $\mathcal{Z}$ and $\mathcal{W}$ for the new infection terms and the remaining transfer terms for y are, respectively, given by

$$\mathcal{Z} = \begin{pmatrix} \lambda\left(\phi_5 R + \phi_1 Q + \phi_2 S + \phi_3 V_1 + \phi_4 V_2\right) \\ 0 \\ 0 \\ 0 \\ 0 \end{pmatrix},$$

and

$$\mathcal{W} = \begin{pmatrix} k_4 E \\ -p\gamma E + k_5 A, \\ -q\gamma E - \pi_2\theta A + k_6 I, \\ -\pi_3\nu I - \psi_2\theta A + k_7 H + \dfrac{\sigma H}{\Phi + H}, \\ -\alpha_1 A - \alpha_2 I + \tau\mathcal{B} \end{pmatrix},$$

Their Jacobian matrices evaluated at $\mathcal{E}_0$ are respectively given by

$$Z = \begin{pmatrix} 0 & \beta_1\frac{N_1}{N_0} & \beta_1\frac{N_1}{N_0} & 0 & \beta_2\frac{N_1}{K} \\ 0 & 0 & 0 & 0 & 0 \\ 0 & 0 & 0 & 0 & 0 \\ 0 & 0 & 0 & 0 & 0 \\ 0 & 0 & 0 & 0 & 0 \end{pmatrix}, \tag{17}$$

and

$$W = \begin{pmatrix} k_4 & 0 & 0 & 0 & 0 \\ -p\gamma & k_5 & 0 & 0 & 0, \\ -q\gamma & -\pi_2\theta & k_6 & 0 & 0, \\ 0 & -\psi_2\theta & -\pi_3\nu & k_7 + \dfrac{\sigma}{\Phi} & 0, \\ 0 & -\alpha_1 & -\alpha_2 & 0 & \tau \end{pmatrix}, \tag{18}$$

with $N_1 = \phi_1 Q_0 + \phi_2 S_0 + \phi_3 V_{10} + \phi_4 V_{20}$. Then, the control reproduction number $\mathcal{R}_c$ is defined, following [7, 57], as the spectral radius of the next generation matrix, ZW^{-1} where

$$ZW^{-1} = \begin{pmatrix} \mathcal{R}_h + \mathcal{R}_e & U_1 & U_2 & 0 & U_3 \\ 0 & 0 & 0 & 0 & 0 \\ 0 & 0 & 0 & 0 & 0 \\ 0 & 0 & 0 & 0 & 0 \\ 0 & 0 & 0 & 0 & 0 \end{pmatrix}.$$

with

$$\begin{aligned} \mathcal{R}_h &= \frac{\beta_1 N_1\left(\pi_2 p\theta + k_5 q\right)\gamma}{k_4 k_5 k_6 N_0} + \frac{\beta_1 p\gamma N_1}{k_4 k_5 N_0} = \frac{\beta_1 N_1\gamma}{k_4 k_5 k_6 N_0}\left[k_8 + k_6 p\right] = \frac{\beta_1 N_1\gamma}{k_4 k_5 k_6 N_0} k_9, \\ \mathcal{R}_e &= \frac{\beta_2 N_1\gamma\left(\alpha_2\left(\pi_2 p\theta + k_5 q\right) + p\alpha_1 k_6\right)}{k_4 k_5 k_6 K\tau} = \frac{\beta_2 N_1\gamma\left(\alpha_2 k_8 + p\alpha_1 k_6\right)}{k_4 k_5 k_6 K\tau} = \frac{\beta_2 N_1\gamma k_{10}}{k_4 k_5 k_6 K\tau}, \\ U_1 &= \frac{\beta_1 K N_1\tau\left(\pi_2\theta + k_6\right) + \beta_2 N_0 N_1\left(\alpha_2\pi_2\theta + \alpha_1 k_6\right)}{k_5 k_6 K N_0\tau}, U_2 = \frac{\beta_1 K N_1\tau + \alpha_2\beta_2 N_0 N_1}{k_6 K N_0\tau}, \\ U_3 &= \frac{\beta_2 N_1}{K\tau}, k_8 = \pi_2 p\theta + k_5 q,\ \ k_9 = k_8 + k_6 p,\ \ k_{10} = \alpha_2 k_8 + p\alpha_1 k_6. \end{aligned} \tag{19}$$

Therefore, the control reproduction number, $\mathcal{R}_c$, is the sum of two main contributions, namely, humans and environment, as follows:

$$\mathcal{R}_c := \rho(ZW^{-1}) = \mathcal{R}_h + \mathcal{R}_e, \tag{20}$$

where $\rho(\bullet)$ represents the spectral radius operator.

The threshold quantity $\mathcal{R}_c$ measures the average number of new Covid-19 infections generated by a single infectious individual in a completely susceptible population where quarantine, treatment and vaccination campaign are implemented [19, 40]. The threshold $\mathcal{R}_h$ represents the number of humans infected through close contact with an infectious individual (either an asymptomatic person (A) or symptomatic person (I_h)) during his/her infectious lifetime. It is equal to the product of the direct contact rate between susceptible individuals and infected individuals, the probability that an exposed human survives the latent period, the average duration of the infectious period in asymptomatic humans, the average duration of the infectious period in symptomatic humans, and the ratio between the total number of persons who will become infected and the total number of humans at the disease-free equilibrium. $\mathcal{R}_e$ represents the number of new infected caused by a contact with an object used by an infected person throughout his/her infectious lifetime. It is equal to the product of the contact rate between susceptible individuals and an object used by an infected individuals, the probability that an exposed human survives the latent period, the average duration of the infectious period in asymptomatic humans, the average duration of the infectious period in symptomatic humans, the natural life expectancy of virus in the environment, the average rate of virus spread to the environment by infectious individuals and the ratio between the total number of persons at the disease-free equilibrium who will become infected, and the total number of free viruses in the environment secreted by an infectious person (A or I).

From [57, Theorem 2], we have the following result.

Lemma 3. *(Local stability of the DFE) The stationary point $\mathcal{E}_0$ of system (13) is locally asymptotically stable (LAS) if $\mathcal{R}_c < 1$, and unstable otherwise.*

2.2.4. Global stability of the DFE

Theorem 4. *The disease-free equilibrium $\mathcal{E}_0$ is globally asymptotically stable in Υ whenever $\mathcal{R}_c < 1$.*

Proof. Considering only the infected compartments of system (13), we obtain

$$\frac{d}{dt}\begin{pmatrix} E(t) \\ A(t) \\ I(t) \\ H(t) \\ \mathcal{B}(t) \end{pmatrix} = (Z - W)\begin{pmatrix} E(t) \\ A(t) \\ I(t) \\ H(t) \\ \mathcal{B}(t) \end{pmatrix} - \mathcal{M}(S, Q, V_1, V_2, E, A, I, H, R, \mathcal{B}), \tag{21}$$

where F and V are the same matrices used to compute the control reproduction number

(see Eq. (20)), and

$$\mathcal{M}(S,Q,V_1,V_2,E,A,I,H,R,\mathcal{B}) = \begin{pmatrix} \beta_1(A+I)\left(\frac{N_1}{N_0}-\frac{\mathcal{N}_1}{N-H}\right)+\beta_2\mathcal{B}\left(\frac{N_1}{K}-\frac{\mathcal{N}_1}{K+\mathcal{B}}\right) \\ 0 \\ 0 \\ 0 \\ 0 \\ 0 \end{pmatrix},$$

where $\mathcal{N}_1 = \phi_2 S + \phi_1 Q + \phi_3 V_1 + \phi_4 V_2 + \phi_5 R$, $N_1 = \phi_2 S_0 + \phi_1 Q_0 + \phi_3 V_{10} + \phi_4 V_{20}$. In Υ, $\frac{N_1}{N_0} \geq \frac{\mathcal{N}_1}{N-H}$ and $\frac{N_1}{K} \geq \frac{\mathcal{N}_1}{K+\mathcal{B}}$ for all $t>0$. Then, it follows that $\mathcal{M}(S,Q,V_1,V_2,E,A,I,H,R,\mathcal{B}) \geq \mathbf{0}_{\mathbb{R}^6}$. This means that

$$\frac{d}{dt}\begin{pmatrix} E(t) \\ A(t) \\ I(t) \\ H(t) \\ \mathcal{B}(t) \end{pmatrix} \leq (Z-W)\begin{pmatrix} E(t) \\ A(t) \\ I(t) \\ H(t) \\ \mathcal{B}(t) \end{pmatrix}.$$

Note that

$$W^{-1} = \begin{pmatrix} \frac{1}{k_4} & 0 & 0 & 0 & 0 \\ \frac{p\gamma}{k_4k_5} & \frac{1}{k_5} & 0 & 0 & 0 \\ \frac{(\pi_2 p\vartheta + k_5 q)\gamma}{k_4k_5k_6} & \frac{\pi_2\vartheta}{k_5k_6} & \frac{1}{k_6} & 0 & 0 \\ \frac{((\pi_2\pi_3\Phi\nu+\varphi_2k_6\Phi)p\vartheta+\pi_3k_5\Phi\nu q)\gamma}{k_4k_5k_6\sigma+k_4k_5k_6k_7\Phi} & \frac{(\pi_2\pi_3\Phi\nu+\varphi_2k_6\Phi)\vartheta}{k_5k_6\sigma+k_5k_6k_7\Phi} & \frac{\pi_3\Phi\nu}{k_6\sigma+k_6k_7\Phi} & \frac{\Phi}{\sigma+k_7\Phi} & 0 \\ \frac{(\alpha_2\pi_2p\vartheta+\alpha_2k_5q+\alpha_1k_6p)\gamma}{k_4k_5k_6\tau} & \frac{\alpha_2\pi_2\vartheta+\alpha_1k_6}{k_5k_6\tau} & \frac{\alpha_2}{k_6\tau} & 0 & \frac{1}{\tau} \end{pmatrix} \geq \mathbf{0}_{\mathbb{R}^{5\times5}}.$$

We also have, from (17), that $Z \geq 0$. Thus, from [51, Theorem 2.1], there exists a Lyapunov function for system (13) expressed as $\mathcal{L}(S,Q,V_1,V_2,E,A,I,H,R,\mathcal{B}) = u'W^{-1}(E,A,I,H,\mathcal{B})'$ where u' is the left eigenvector of the nonnegative matrix $W^{-1}Z$ corresponding to the eigenvalue $\mathcal{R}_c$. This implies that,

$$\frac{d\mathcal{L}}{dt} = (\mathcal{R}_c - 1)\,u'(E,A,I,H,\mathcal{B}) - u'W^{-1}\mathcal{M}(S,Q,V_1,V_2,E,A,I,H,R,\mathcal{B}) \leq 0.$$

Since $\mathcal{M}(S,Q,V_1,V_2,E,A,I,H,R,\mathcal{B}) \geq \mathbf{0}_{\mathbb{R}^5}$, it follows that $\frac{d\mathcal{L}}{dt} < 0$ whenever $\mathcal{R}_c < 1$, with $\frac{d\mathcal{L}}{dt} = 0$ if and only if $(E,A,I,H,\mathcal{B}) = \mathbf{0}_{\mathbb{R}^5}$. It follows that the largest invariant set contained in $\left\{(S,Q,V_1,V_2,E,A,I,H,R,\mathcal{B}) \in \mathbb{R}^{10}_+ : \frac{d\mathcal{L}}{dt} = 0\right\}$ is $\{\mathcal{E}_0\}$. Thus, from LaSalle Invariance Principle [29], every solution of (13) with initials conditions in Υ converge to $\mathcal{E}_0$ when $t \longrightarrow +\infty$. That is $(E,A,I,H,\mathcal{B}) \longrightarrow (0,0,0,0,0)$, $S \longrightarrow S_0$, $Q \longrightarrow Q_0$, $V_1 \longrightarrow V_{10}$ and $V_2 \longrightarrow V_{20}$ when $t \longrightarrow +\infty$, which is equivalent to $(S,Q,V_1,V_2,E,A,I,H,R,\mathcal{B}) \longrightarrow (S_0,Q_0,V_{10},V_{20},0,0,0,0,0,0)$ when $t \longrightarrow +\infty$. Thus, the disease-free equilibrium $\mathcal{E}_0$ is globally asymptotically stable in $\mathcal{W}$ whenever $\mathcal{R}_c < 1$. This ends the proof. □

2.2.5. Existence of endemic equilibrium points

Due to the model complexity, we consider only the particular case when $\sigma = 0$ and $\phi_i = 1$ for $i \in 1, 2, 3, 4$. $\sigma = 0$ implies that there are no specific medical resources supplied which was the case at the beginning of the Covid-19 epidemic in Wuhan, China. $\phi_1 = \phi_2 = \phi_3 = \phi_4 = 1$ implies that susceptible individuals, as well as quarantined, and vaccinated individuals, have the same probability to become infected and the vaccine does not confer immunity. This is motivated by the fact that, in the case of the Covid-19 pandemic, available vaccines do not confer permanent immunity, but permit the reduction of the number of critical cases by the decrease the number of Covid-19 hospitalization as well as the number of deaths due to the Covid-19 pandemic [15].

We claim:

Proposition 1. *Assume that $\mathcal{R}_c > 1$ or $\mathcal{R}_c \leq 1$. Then, in addition to the disease-free equilibrium $\mathcal{E}_0$, the Covid-19 model could have one or more than one positive equilibrium.*

Proof. See Appendix D. □

The case $\mathcal{R}_c < 1$ of Proposition 1 suggests the possibility that the forward (resp. backward) bifurcation phenomenon can occurs in the Covid-19 model (13). Since from Theorem 4, the disease-free equilibrium is globally asymptotically stable, it follows that even if the DFE co-exists with other positive equilibrium points in Υ, these last are unstable.

3. Model calibration and sensitivity analysis

3.1. Model calibration with real data of Germany

The start date of mass vaccination in Germany was Sunday, 27 December 2020 [17]. Since then, several constrained measures was taken to ensure that the majority of inhabitants is vaccinated. We consider the daily infected reported cases in Germany from February 15, 2021 to April 05, 2021 [22]. The map of the Federal Republic of Germany is depicted in Figure 1. Taking the total approximate population of Germany equal to $N(0) = 83,000,000$ [18], the recruitment rate is equal to $\Lambda = \mu N(0)$. The following initial conditions subject to the data fitting ar $S(0) = 48,790,644$ and the other variables with the initial conditions subject to data fitting are $Q(0) = 2,338,987$, $V_1(0) = 23,240,000$, $V_2(0) = 2,324,000$, $E(0) = 2,32,843$, $A(0) = 0$, $I(0) = 2,338,987$, $H(0) = 23,389$, $R(0) = 160,115$, and $B(0) = 10^6$. The nonlinear square method is used to fit the model to the real data. It provides realistic values of model parameters, which is beneficial when we want to forecast the evolution of the disease in a given time interval. We perform experiments until the desired accurate fitting of the model is achieved. After solving numerically the following optimization problem

$$\min_{\Gamma} \parallel I_{\text{predict}} - I_{\text{data}} \parallel_2, \tag{22}$$

where $\Gamma = \{\beta_1, \beta_2, v_1, v_2, c_1, c_2, \gamma, \theta, \psi_1, \psi_2\}$, we obtain the results consigned in Table 2. The value of the control reproduction number computed with the parameter values in Table 2 is $\mathcal{R}_c = 1.899451294774579$. The model simulations versus data fitting are depicted in Figure 2. The future evolution of the disease without any added control measures is depicted in Figure 3. It is clear that, in a long term, the disease will persist in the population if there is no best scientific advance like, for example, the establishment of a vaccine that could protect a vaccinated person to be infected, even if this vaccinated person has close contact with the virus or a sick person. For the moment, available vaccines permit only to prevent severe

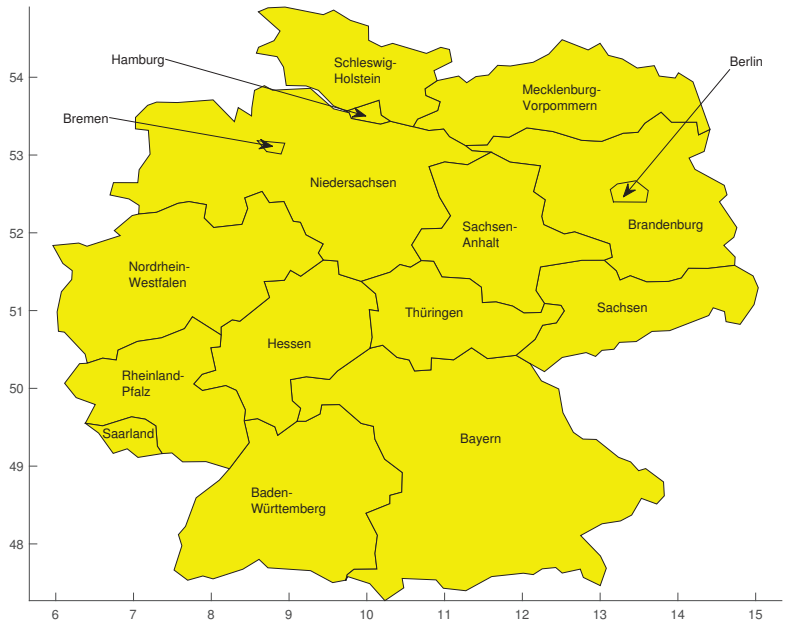

Figure 1: Map of the Federal Republic of Germany with its sixteen states.

Table 2: Model parameters and their estimated values.

Parameter	Value/per day	Source	Parameter	Value/per day	Source
Λ	$N(0) \times \mu$	Estimated	ζ	0.1428	[55]
μ	$\frac{1}{81.72 \times 365}$	Estimated	α_1	0.1	[39]
β_1	0.052428772948116	Fitted	α_2	0.1	[39]
β_2	3.303061249323349e-07	Fitted	τ	0.1724	[39]
r_1	0.1	Assumed	K	10^6	[11]
r_2	0.8	Assumed	δ_1	0.0018	[39]
r_3	0.05	Assumed	δ_2	0.0018	[39]
v_1	0.000547888192948	Fitted	q	0.7	[39]
v_2	0.000080792493821	Fitted	η	0.09	[39]
c_1	0.000318771165360	Fitted	σ	0.0584	[48]
c_2	0.014228191665571	Fitted	Φ	3.0173	[48]
γ	0.759448007021108	Fitted	ϕ_1	0.596	[40]
θ	0.019286496666118	Fitted	ϕ_2	1	Assumed
ψ_1	0.31	Assumed	ϕ_3	0.52	[14]
ψ_2	0.045	Assumed	ϕ_4	0.52	[14]
ν	0.017	Assumed	ϕ_5	0.5	Assumed

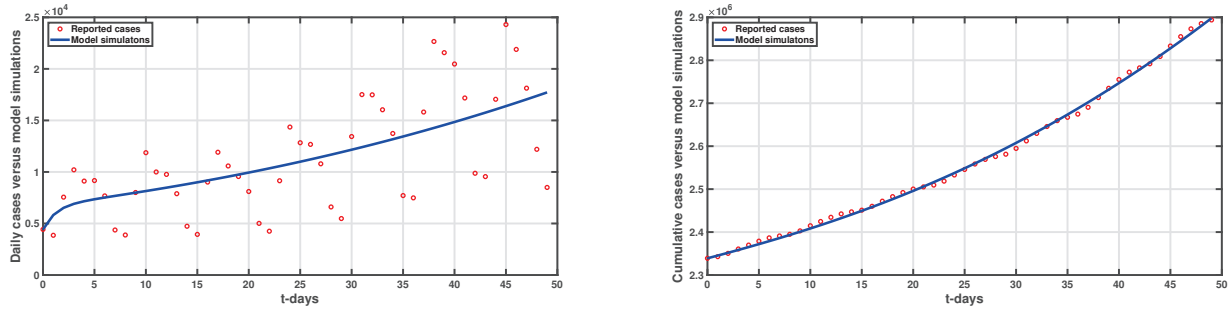

(a) Daily reported cases (b) Cumulative reported cases

Figure 2: Model fitting versus reported cases in Germany during the period from February 15, 2021 ($t = 0$) to April 05, 2021 ($t = 49$).

forms of the disease by decreasing the number of hospitalized cases as well as the number of deaths.

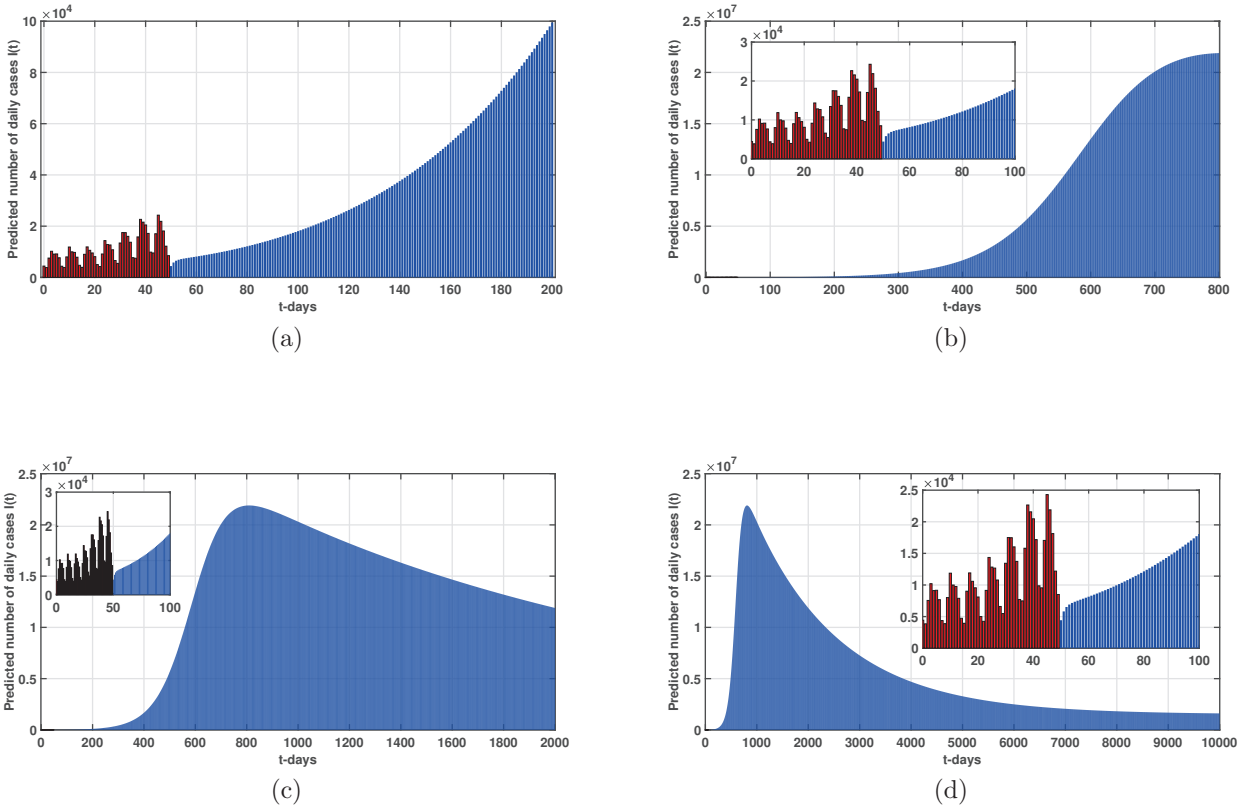

(a) (b)

(c) (d)

Figure 3: Short and Long-term forecasting of Coronavirus (Covid-19) pandemic in Germany.

The impact of the vaccination process is depicted on Figure 4 by varying the vaccination coverage between 0 and 70%. The simulation results show that vaccination forward delayed the date of the epidemic peak. Whatever the vaccine coverage, the dynamics of the disease remain the same after the epidemic peak. This can be justify by the fact that the available Covid-19 vaccines do not prevent the virus transmission between infectious persons and

vaccinated persons. This is why it is urgent to develop a Covid-19 vaccine which prevents virus transmission with a high efficacy level.

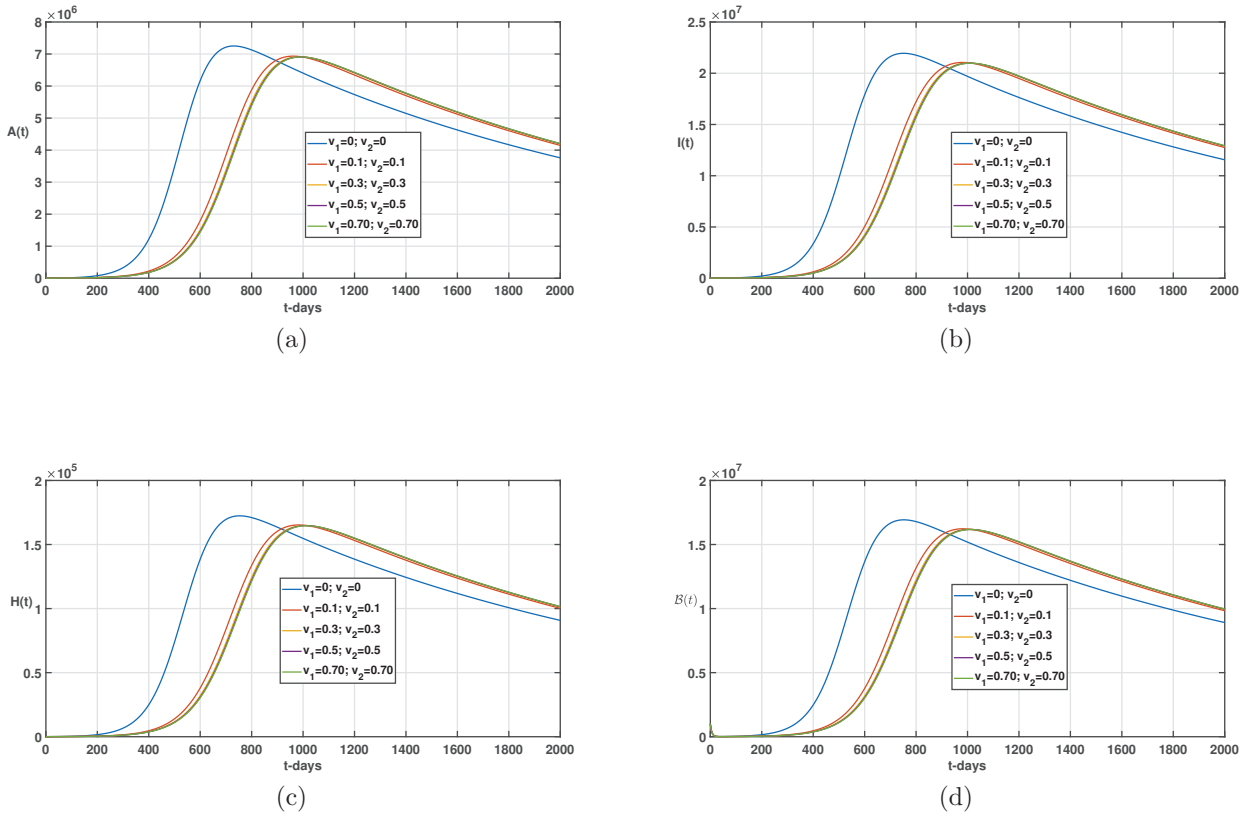

Figure 4: Impact of vaccination coverage on the Covid-19 dynamics in Germany.

Now, we fix the vaccine coverage at 70%, that is $v_1 = v_2 = 0.7$, and varying the vaccine efficacy at the second dose between 0 to 100%, that is $\phi_4 \in \{0, 0.52, 0.75, 0.95\}$. The result, depicted on Figure 5, shows that fight against Covid-19 pandemic passes through by intensification of vaccination campaigns with a vaccine with a high efficacy level.

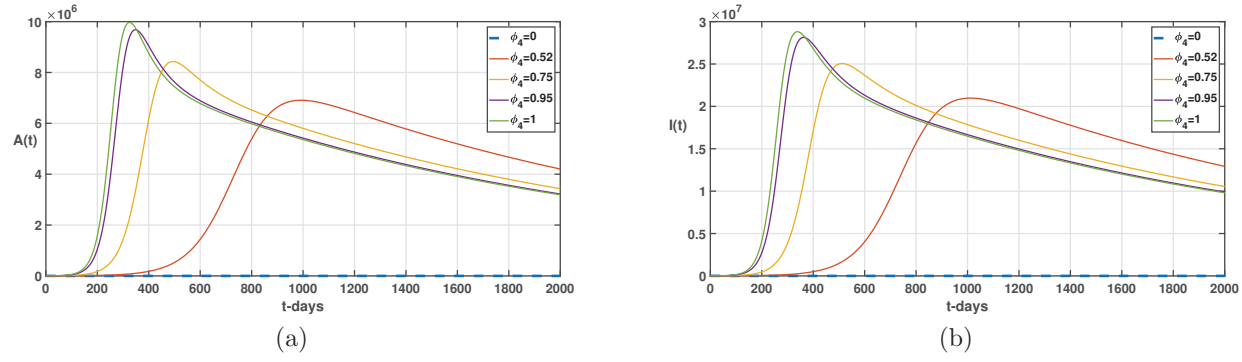

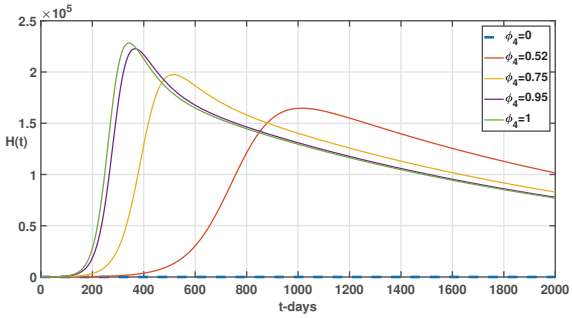

(c)

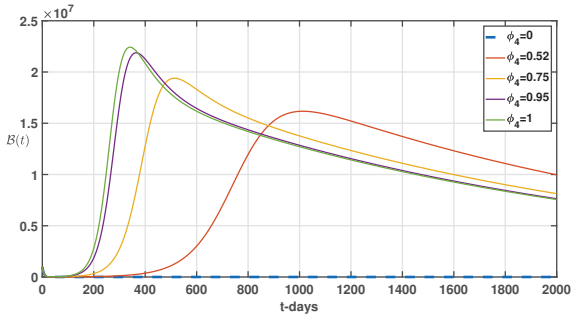

(d)

Figure 5: Impact of vaccine efficacy on the Covid-19 dynamics in Germany with a fixed vaccine coverage equal to 70%.

3.2. Uncertainty and global Sensitivity analysis

Using 10,000 runs of the Latin hypercube sampling (LHS) [53], we compute the partial rank correlation coefficients (PRCC) between the control reproduction number $\mathcal{R}_c$ and each model parameters [1, 33, 63]. Each model parameter is supposed to be a random variable, uniformly distributed, with its mean value as listed in Table 2. With this 10,000 sampling, we obtain the mean value of $\mathcal{R}_c$ equal to 2.4724 which implies that we are in an endemic state. The derived distribution of $\mathcal{R}_c$ is depicted in Figure 6 (panel (a)) while the PRCCs are depicted in panel (b) of Figure 6. Statistically, a large PRCC value ($> +0.5$ or < -0.5) with less P-values (< 0.001) indicates that the corresponding parameter is influency in the model dynamics. It then follows that β_1, the human-to-human transmission probability, and ϕ_2, a modification parameter which indicates the level of infectiousness of susceptible individuals, are the most influential for the control reproduction number $\mathcal{R}_c$.

Figure 7 depicts PRCC between infected states E, A, I and H, and each model parameter, as well as the corresponding P-values. We observe that: For the compartment E, the most influence parameters are β_1, γ and ϕ_2; For the compartment A, the most influence parameters are β_1, θ, q and ϕ_2; For the compartment I, the most influence parameters are β_1, ν and ϕ_2; And for the compartment H, the most influence parameters are β_1, ν, η and ζ. This suggest that control measures like individual protection, prevention and treatment (with high level of efficacy) combined with all measures which consist to detect new cases as well as which can boost the immunity system must be intensified to fight against the persistence of Covid-19 in the population.

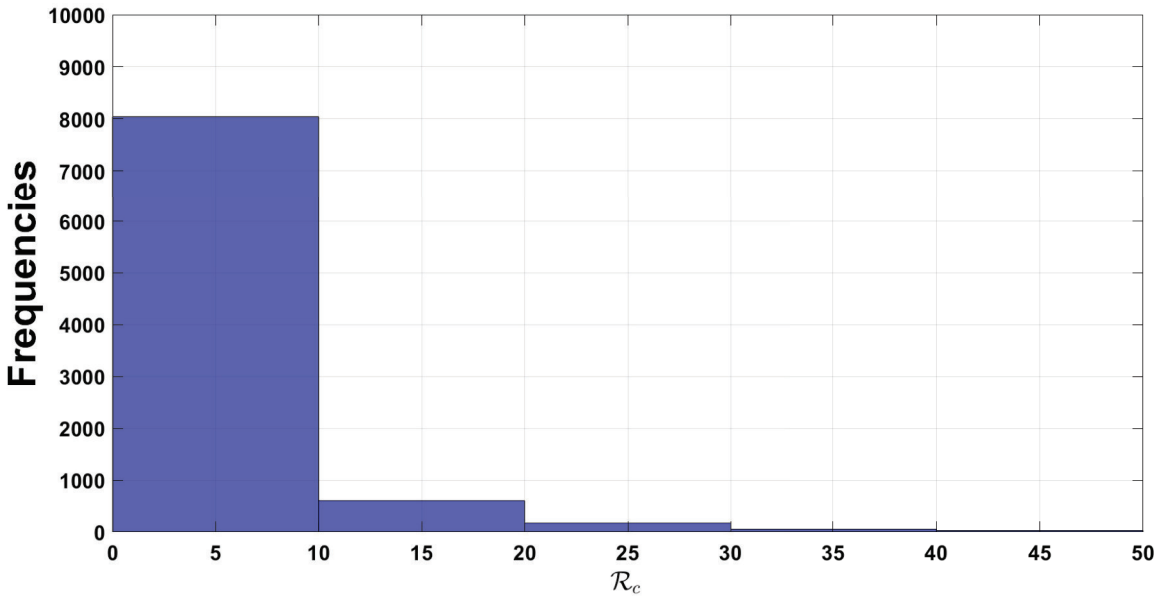

(a) Sampling distribution of $\mathcal{R}_c$ from 10,000 runs of Latin hypercube sampling.

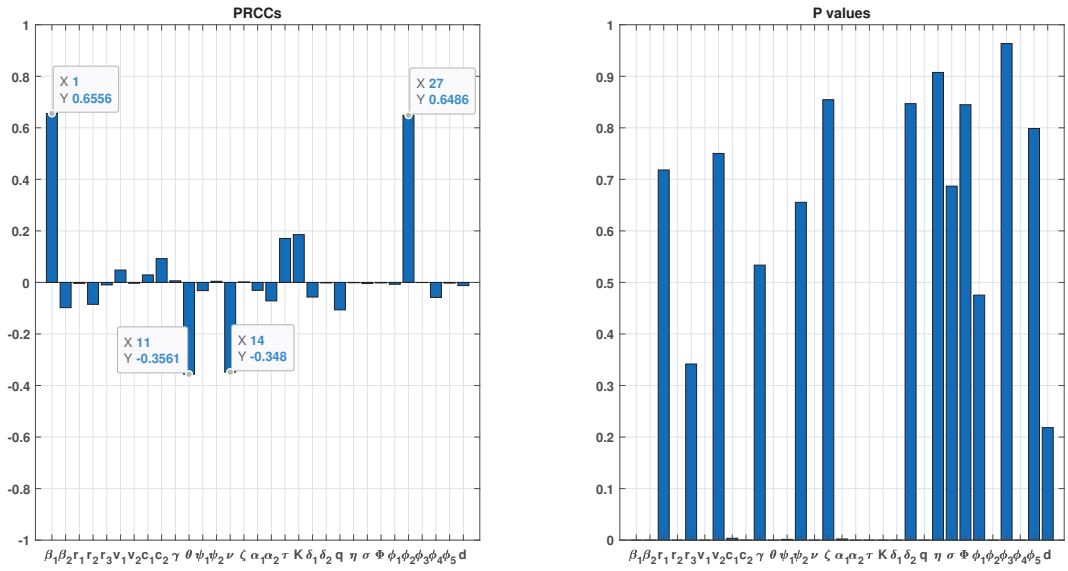

(b) PRCCs between $\mathcal{R}_c$ and model parameters

Figure 6: Sampling distribution of $\mathcal{R}_c$ (a) and global sensitivity indices (b) for $\mathcal{R}_c$ against model parameters. The character 'd' stands for the dummy parameter.

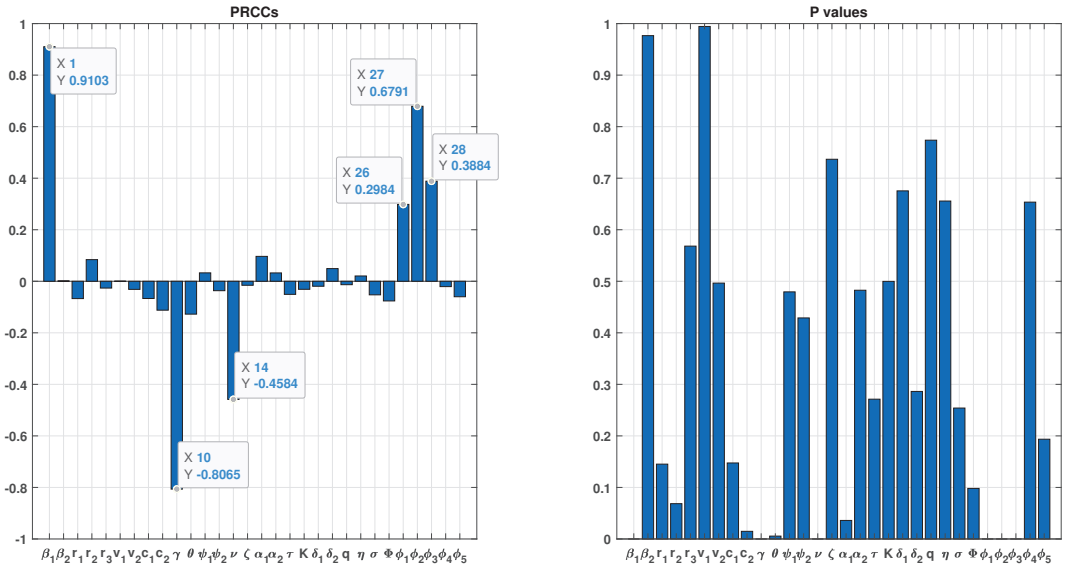

(a) PRCCs between the infected compartment E and model parameters

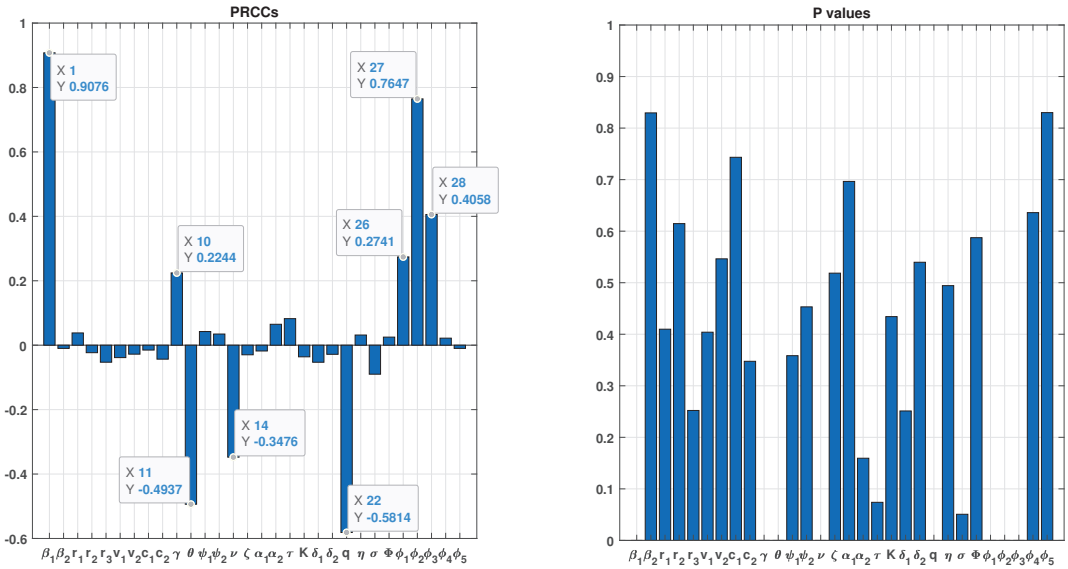

(b) PRCCs between the infected compartment A and model parameters

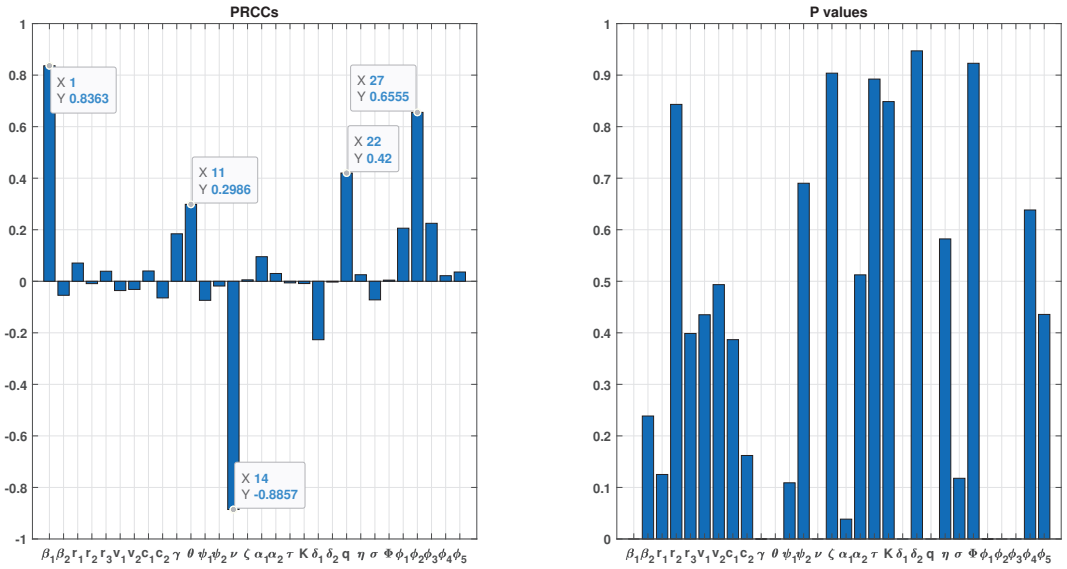

(c) PRCCs between the infected compartment I and model parameters

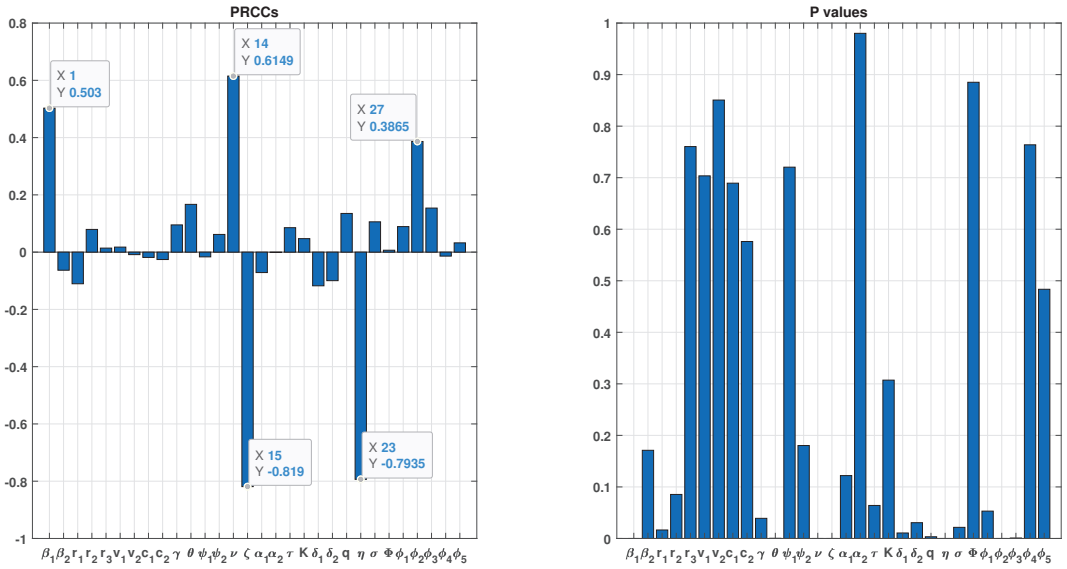

(d) PRCCs between the infected compartment H and model parameters

Figure 7: Global sensitivity indices for infected state variables of the model (13) against model parameters.

Figures 8 shows the control reproduction number $\mathcal{R}_c$ as a function of some model parameters. In panel (a) of Figure 8, $\mathcal{R}_c$ is represented as a function of the direct transmission contact coefficient β_1 and the indirect transmission contact coefficient β_2. We see that $\mathcal{R}_c$ increases rapidly according to the increase of β_1 than β_2. This suggests that decreasing the coefficient β_1 is the best way to reduce the control reproduction number. In panel (b) of Figure 8, $\mathcal{R}_c$ is represented as a function of the coefficients β_1 and ζ. It clear from panel (b) of Figure 8 that $\mathcal{R}_c$ increases rapidly according to the increase of β_1 and the decrease of ζ. This suggest that individual protection combined with effective treatment can permits to

reduce the control reproduction number.

In panel (c) of Figure 8, $\mathcal{R}_c$ is represented as a function of the coefficients β_1 and ϕ_2. By Noting that $\phi_2 = 1 - \epsilon_2$ where ϵ_2 represents the booster immunity level, we look that decreasing simultaneously these two parameters permits to decrease $\mathcal{R}_c$, that is, not individual protection with a population with weakened immune system contributes to the persistence of the disease in the population. In panel (d) of Figure 8, $\mathcal{R}_c$ is represented as a function of the coefficients β_1 and γ. We see $\mathcal{R}_c$ is a increase function of this two parameters. The same way is observed in the remaining panels (e) and (f).

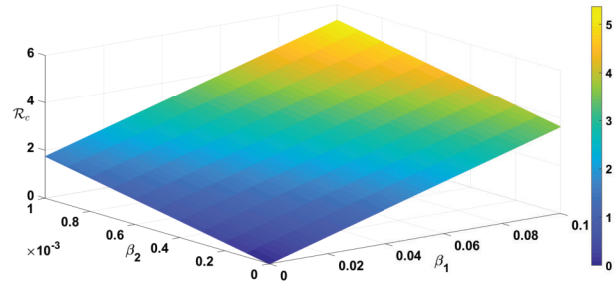

(a) 3-D plot of $\mathcal{R}_c$ as a function of β_1 and β_2

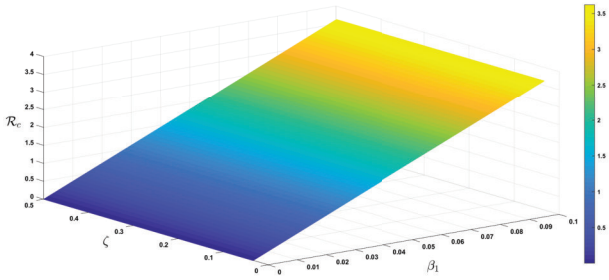

(b) 3-D plot of $\mathcal{R}_c$ as a function of β_1 and ζ

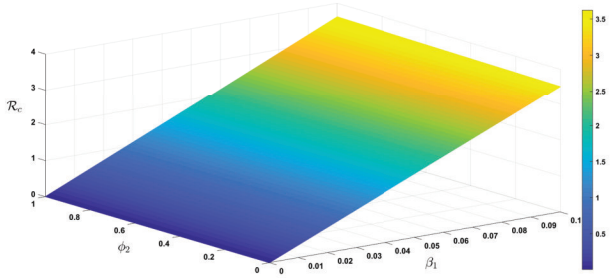

(c) 3-D plot of $\mathcal{R}_c$ as a function of β_1 and ϕ_2

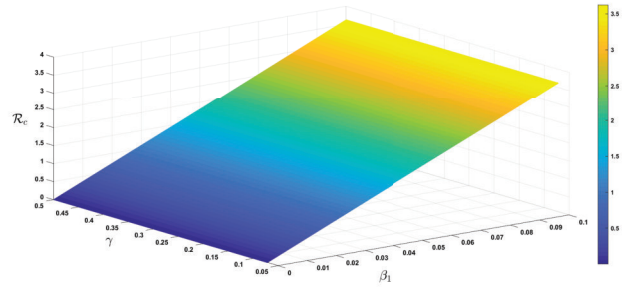

(d) 3-D plot of $\mathcal{R}_c$ as a function of β_1 and γ

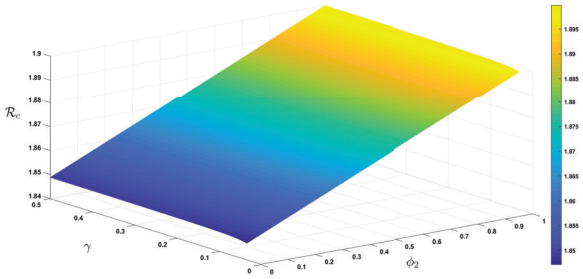

(e) Contour plot of $\mathcal{R}_c$ as a function of ϕ_2 and γ

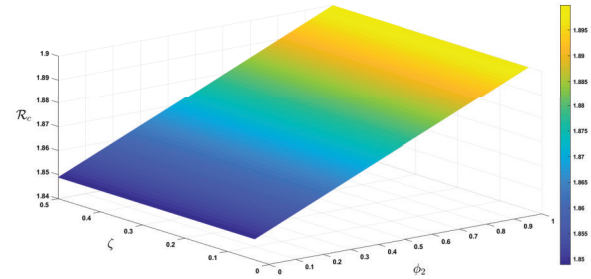

(f) Contour plot of $\mathcal{R}_c$ as a function of ϕ_2 and ζ

Figure 8: 3-D plot of $\mathcal{R}_c$ as a function of some model parameters. The parameter values are those of Table 2 except (a) β_1 and β_2; (b) $beta_1$ and ζ; (c) β_1 and ϕ_2; (d) β_1 and γ; (e) ϕ_2 and γ; (f) ϕ_2 and ζ which vary.

4. The fractional model

4.1. Preliminary definitions and results

Definition 1 (The R-L integral). *Let $f \in L^1([0;a],\mathbb{R}_+)$, $a>0$. The fractional order integral of f of order $\varphi>0$, in the sense of Riemann-Liouville, is defined as*

$$ {}_a^C\mathcal{I}_t^{\varphi}\left(f(t)\right) = \frac{1}{\Gamma(\varphi)}\int_0^t f(\theta)(t-\theta)^{\varphi-1}d\theta. \tag{23}$$

Definition 2 (The Caputo derivative [45]). *Let $f \in \mathcal{C}^m([0;a])$, $a>0$, $\varphi\in\mathbb{R}$, $m\in\mathbb{N}$ such that $m-1<\varphi<m$. The Caputo fractional order derivative of f of order φ is defined as*

$$ {}_a^C\mathcal{D}_t^{\varphi}\left(f(t)\right) = \frac{1}{\Gamma(\varphi-m)}\int_a^t (t-\theta)^{m-\varphi-1} f^{(m)}(\theta)\,d\theta, \quad t>0. \tag{24}$$

Definition 3 (The Mittag-Leffler function [36]). *The Mittag-Leffler function of order $\varphi>0$ is an entire function defined by the series*

$$ \mathbf{E}_{\varphi}(x) = \sum_{k=0}^{\infty}\frac{x^k}{\Gamma(\varphi k+1)}. \tag{25}$$

4.2. The fractional model and its analysis

The new formulation of the Covid-19 transmission model (13) with the Caputo fractional derivative is given by

$$\begin{cases}
{}_a^C\mathcal{D}_t^{\varphi}S(t) &= r_2\Lambda^{\varphi} + c_1^{\varphi}Q(t) - \left(k_1^{\varphi}+\phi_2\lambda(t)\right)S(t),\\
{}_a^C\mathcal{D}_t^{\varphi}Q(t) &= r_1\Lambda^{\varphi} + c_2^{\varphi}S(t) - \left(k_2^{\varphi}+\phi_1\lambda(t)\right)Q(t),\\
{}_a^C\mathcal{D}_t^{\varphi}V_1(t) &= r_3\Lambda^{\varphi} + v_1^{\varphi}S(t) - \left(k_3^{\varphi}+\phi_3\lambda(t)\right)V_1(t),\\
{}_a^C\mathcal{D}_t^{\varphi}V_2(t) &= \pi_1\Lambda^{\varphi} + v_2^{\varphi}V_1(t) - \left(\mu^{\varphi}+\phi_4\lambda(t)\right)V_2(t),\\
{}_a^C\mathcal{D}_t^{\varphi}E(t) &= \lambda(t)\left(\phi_5R(t)+\phi_1Q(t)+\phi_2S(t)+\phi_3V_1(t)+\phi_4V_2(t)\right) - k_4^{\varphi}E(t),\\
{}_a^C\mathcal{D}_t^{\varphi}A(t) &= p\gamma^{\varphi}E(t) - k_5^{\varphi}A(t),\\
{}_a^C\mathcal{D}_t^{\varphi}I(t) &= q\gamma^{\varphi}E(t) + \pi_2\theta^{\varphi}A(t) - k_6^{\varphi}I(t),\\
{}_a^C\mathcal{D}_t^{\varphi}H(t) &= \pi_3\nu^{\varphi}I(t) + \psi_2\theta^{\varphi}A(t) - k_7^{\varphi}H(t) - \mathcal{T}(\sigma,H(t)),\\
{}_a^C\mathcal{D}_t^{\varphi}R(t) &= \psi_1\theta^{\varphi}A(t) + \eta\nu^{\varphi}I(t) + \zeta^{\varphi}H(t) + \mathcal{T}(\sigma,H(t))(t) - \left(\mu^{\varphi}+\phi_5\lambda(t)\right)R(t),\\
{}_a^C\mathcal{D}_t^{\varphi}\mathcal{B}(t) &= \alpha_1^{\varphi}A(t) + \alpha_2^{\varphi}I(t) - \tau^{\varphi}\mathcal{B}(t).
\end{cases} \tag{26}$$

where

$$ \lambda(t) = \beta_1^{\varphi}\frac{A(t)+I(t)}{N(t)-H(t)} + \beta_2^{\varphi}\frac{\mathcal{B}(t)}{K+\mathcal{B}(t)}, \quad \text{and} \quad \mathcal{T}(\sigma,H(t))(t) = \frac{\sigma^{\varphi}H(t)}{\Phi+H(t)}, \tag{27}$$

and $k_1^{\varphi} = \mu^{\varphi}+c_2^{\varphi}+v_1^{\varphi}$, $k_2^{\varphi} = \mu^{\varphi}+c_1^{\varphi}$, $k_3^{\varphi} = \mu^{\varphi}+v_2^{\varphi}$, $k_4^{\varphi} = \mu^{\varphi}+\gamma^{\varphi}$, $k_5^{\varphi} = \mu^{\varphi}+\theta^{\varphi}$, $k_6^{\varphi} = \mu^{\varphi}+\delta_1^{\varphi}+\nu^{\varphi}$, $k_6^{\varphi} = \mu^{\varphi}+\delta_2^{\varphi}+\zeta^{\varphi}$.

For dimensional consistency emphasized by Diethelm in [8], all model parameters except r_1, r_2, r_3, q, ψ_1, ψ_2, η, and ϕ_i for $i\in[1;5]\cap\mathbb{N}$ have dimensions $\frac{1}{t^{\varphi}}$.

System (26) is subject to the following initial conditions

$$\begin{aligned}
&S(0)=S_0>0, Q(0)=Q_0\geq 0, V_1(0)=V_{10}\geq 0, V_2(0)=V_{20}\geq 0, E(0)=E_0\geq 0,\\
&A(0)=A_0\geq 0, I(0)=I_0\geq 0, H(0)=H_0\geq 0, R(0)=R_0\geq 0, \mathcal{B}(0)=\mathcal{B}_0\geq 0.
\end{aligned} \tag{28}$$

Let us set $x = (S, Q, V_1, V_2, E, A, I, H, R, \mathcal{B}(t))'$ and $\mathbb{K}(t, x(t)) = (f_i^{\varphi})'$, $i \in [0, 10] \cap \mathbb{N}$, where f_i^{φ} for $i \in [0, 10] \cap \mathbb{N}$ are the right-hand side of system (26). Thus the fractional model (26) is rewritten in the following compact form

$$ {}_a^C\mathcal{D}_t^{\varphi} x(t) = \mathbb{K}(t, x(t)), \quad x(0) = x_0 \geq 0, \quad t \in [0, a], \quad a > 0, \quad 0 < \varphi \leq 1, \tag{29} $$

with the condition $x(0) = x_0 \geq 0$ which is interpreted component by component.

The initial value problem (IVP) is in turn rewritten in the following integral form

$$ x(t) = x(0) + {}_a^C\mathcal{I}_t^{\varphi} \left(\mathbb{K}(t, x(t)) \right). \tag{30} $$

The following results hold. The proofs are obtained as the same ways than the results obtained for the model (13).

Theorem 5. *For $x(t) \geq \mathbf{0}_{\mathbb{R}^{10}}$, the solution $x(t)$ of the IVP (29) is positive whenever $t \geq 0$.*

Let us define the following subset of $\mathbb{R}_+^{10}$

$$ \Upsilon^{\varphi} = \left\{ x = (S, Q, V_1, V_2, E, A, I, H, R, \mathcal{B})' \in \mathbb{R}_+^{10} : \left(\sum_{i=1}^{9} x_i \right) \leq \frac{\Lambda^{\varphi}}{\mu^{\varphi}}, \quad x_{10} \leq \frac{(\alpha_1^{\varphi} + \alpha_2^{\varphi})\Lambda^{\varphi}}{\mu^{\varphi}\tau^{\varphi}} \right\}. \tag{31} $$

Theorem 6. *(Boundedness of solutions)*
The region Υ^{φ} is positively invariant and attracting for system (26).

Lemma 4. *The function $\mathbb{K} : [0; \infty) \times \mathbb{R}^{10} \to \mathbb{R}^{10}$ defined in (29) is a continuously differentiable function on $\mathbb{R}^{10}$.*

Lemma 5. *The continuously differentiable function $\mathbb{K} : [0; \infty) \times \mathbb{R}^{10} \to \mathbb{R}^{10}$ defined in (29) is locally Lipschitz continuous on $\mathbb{R}^{10}$.*

Theorem 7 (Existence-uniqueness)**.** *For initial conditions $x_0 = (S_0, Q_0, V_{10}, V_{20}, E_0, A_0, I_0, H_0, R_0, B_0)' \in \mathbb{R}_+^{10}$, the Covid-19 transmission model (26) admits a unique solution $x \in \mathcal{C}([0; +\infty[, \mathbb{R}_+^{10})$.*

4.2.1. Steady states and stability analysis

4.2.2. Local stability of the disease-free equilibrium

As for the case of the model with integer derivative (13), the fractional model (26) admits always one stationary point, also called disease-free equilibrium (DFE), $\mathcal{E}_0 = (S_0, Q_0, V_{10}, V_{20}, 0, 0, 0, 0, 0, 0)'$ where

$$ \begin{cases} S_0 &= \dfrac{\left[c_1^{\varphi}\left(c_2^{\varphi} r_2 + k_1^{\varphi} r_1\right) + \left(k_1^{\varphi} k_2^{\varphi} - c_1^{\varphi} c_2^{\varphi}\right) r_2\right] \Lambda^{\varphi}}{k_1^{\varphi}\left(k_1^{\varphi} k_2^{\varphi} - c_1^{\varphi} c_2^{\varphi}\right)}, \\ Q_0 &= \dfrac{\left(c_2^{\varphi} r_2 + k_1^{\varphi} r_1\right) \Lambda^{\varphi}}{k_1^{\varphi} k_2^{\varphi} - c_1^{\varphi} c_2^{\varphi}}, \\ V_{10} &= \dfrac{\left[\left(k_1 k_2 - c_1 c_2\right) r_3 + v_1^{\varphi}\left(k_2^{\varphi} r_2 + c_1^{\varphi} r_1\right)\right] \Lambda^{\varphi}}{\left(k_1^{\varphi} k_2^{\varphi} - c_1^{\varphi} c_2^{\varphi}\right) k_3^{\varphi}}, \\ V_{20} &= \dfrac{\left[\left(k_1^{\varphi} k_2^{\varphi} - c_1^{\varphi} c_2^{\varphi}\right)\left(v_2^{\varphi} r_3^{\varphi} + \pi_1 k_3^{\varphi}\right) + \left(k_2^{\varphi} r_2 + c_1^{\varphi} r_1\right) v_1^{\varphi} v_2^{\varphi}\right] \Lambda^{\varphi}}{\left(k_1^{\varphi} k_2^{\varphi} - c_1^{\varphi} c_2^{\varphi}\right) k_3^{\varphi} \mu}. \end{cases} \tag{32} $$

with $k_1^{\varphi} k_2^{\varphi} - c_1^{\varphi} c_2^{\varphi} = (\mu^{\varphi})^2 + \left(c_2^{\varphi} + v_1^{\varphi} + c_1^{\varphi}\right)\mu^{\varphi} + c_1^{\varphi} v_1^{\varphi} > 0$. From (16), we have $N_0 := S_0 + Q_0 + V_{10} + V_{20} = \dfrac{\Lambda^{\varphi}}{\mu^{\varphi}}$.

As in the case of the ODE model (13), we compute the control reproduction number, denoted by $\mathcal{R}_c$ using the next generation approach (see [7, 57]), and the control reproduction number of the fractional model (26) is given by

$$\mathcal{R}_c = \frac{\beta_1^\varphi N_1 \gamma^\varphi k_9^\varphi}{k_4^\varphi k_5^\varphi k_6^\varphi N_0} + \frac{\beta_2^\varphi N_1 \gamma^\varphi k_{10}^\varphi}{k_4^\varphi k_5^\varphi k_6^\varphi \tau^\varphi K}. \tag{33}$$

Before study the local stability of the disease-free equilibrium, let us recall the following result.

Lemma 6. *[21, Theorem 4.4] The disease-free equilibrium of the fractional model (26) is locally asymptotically stable if all the eigenvalues ϖ_i of its Jacobian matrix evaluated at the DFE satisfy $|\arg(\varpi_i)| > \frac{\varphi\pi}{2}$, $i = [1; 10] \cap \mathbb{N}$.*

The Jacobian of system (26) evaluated at the disease-free equilibrium $\mathcal{E}_0$ is given by

$$\mathcal{J}(\mathcal{E}_0) = \begin{pmatrix}
-k_1^\varphi & c_1 & 0 & 0 & 0 & -\beta_1^\varphi \phi_2 \frac{S_0}{N_0} & -\beta_1^\varphi \phi_2 \frac{S_0}{N_0} & 0 & 0 & -\beta_2^\varphi \phi_2 \frac{S_0}{K} \\
c_2^\varphi & -k_2^\varphi & 0 & 0 & 0 & -\beta_1^\varphi \phi_1 \frac{Q_0}{N_0} & -\beta_1^\varphi \phi_1 \frac{Q_0}{N_0} & 0 & 0 & -\beta_2^\varphi \phi_1 \frac{Q_0}{K} \\
v_1^\varphi & 0 & -k_3^\varphi & 0 & 0 & -\beta_1^\varphi \phi_3 \frac{V_{10}}{N_0} & -\beta_1^\varphi \phi_3 \frac{V_{10}}{N_0} & 0 & 0 & -\beta_2^\varphi \phi_3 \frac{V_{10}}{K} \\
0 & 0 & v_2^\varphi & -\mu^\varphi & 0 & -\beta_1^\varphi \phi_4 \frac{V_{20}}{N_0} & -\beta_1^\varphi \phi_4 \frac{V_{20}}{N_0} & 0 & 0 & -\beta_2^\varphi \phi_4 \frac{V_{20}}{K} \\
0 & 0 & 0 & 0 & -k_4^\varphi & \beta_1^\varphi \frac{N_1}{N_0} & \beta_1^\varphi \frac{N_1}{N_0} & 0 & 0 & \beta_2^\varphi \frac{N_1}{K} \\
0 & 0 & 0 & 0 & p\gamma^\varphi & -k_5^\varphi & 0 & 0 & 0 & 0 \\
0 & 0 & 0 & 0 & q\gamma^\varphi & \pi_2 \theta^\varphi & -k_6^\varphi & 0 & 0 & 0 \\
0 & 0 & 0 & 0 & 0 & \psi_2 \theta^\varphi & \pi_3 \nu^\varphi & -k_7^\varphi - \frac{\sigma^\varphi}{\Phi} & 0 & 0 \\
0 & 0 & 0 & 0 & 0 & \psi_1 \theta^\varphi & \eta \nu^\varphi & \zeta^\varphi + \frac{\sigma^\varphi}{\Phi} & -\mu^\varphi & 0 \\
0 & 0 & 0 & 0 & 0 & \alpha_1^\varphi & \alpha_2^\varphi & 0 & 0 & -\tau^\varphi
\end{pmatrix}.$$

The eigenvalues of $\mathcal{J}(\mathcal{E}_0)$ are $-\mu^\varphi$, $-k_3^\varphi$, $-\left(k_7^\varphi + \frac{\sigma^\varphi}{\Phi}\right)$, and those of the following sub-matrix

$$\mathcal{J}_1 = \begin{pmatrix}
-k_1^\varphi & c_1^\varphi & 0 & -\beta_1^\varphi \phi_2 \frac{S_0}{N_0} & -\beta_1^\varphi \phi_2 \frac{S_0}{N_0} & -\beta_2^\varphi \phi_2 \frac{S_0}{K} \\
c_2^\varphi & -k_2^\varphi & 0 & -\beta_1^\varphi \phi_1 \frac{Q_0}{N_0} & -\beta_1^\varphi \phi_1 \frac{Q_0}{N_0} & -\beta_2^\varphi \phi_1 \frac{Q_0}{K} \\
0 & 0 & -k_4^\varphi & \beta_1^\varphi \frac{N_1}{N_0} & \beta_1^\varphi \frac{N_1}{N_0} & \beta_2^\varphi \frac{N_1}{K} \\
0 & 0 & p\gamma^\varphi & -k_5^\varphi & 0 & 0 \\
0 & 0 & q\gamma^\varphi & \pi_2 \theta^\varphi & -k_6^\varphi & 0 \\
0 & 0 & 0 & \alpha_1^\varphi & \alpha_2^\varphi & -\tau^\varphi
\end{pmatrix} = \begin{pmatrix} \mathcal{J}_{11} & \bullet \\ \mathbf{0}_{\mathbb{R}^{4\times 2}} & \mathcal{J}_{22} \end{pmatrix}.$$

with

$$\mathcal{J}_{11} = \begin{pmatrix} -k_1^\varphi & c_1^\varphi \\ c_2^\varphi & -k_2^\varphi \end{pmatrix},$$

and

$$\mathcal{J}_{22} = \begin{pmatrix}
-k_4^\varphi & \beta_1^\varphi \frac{N_1}{N_0} & \beta_1^\varphi \frac{N_1}{N_0} & \beta_2^\varphi \frac{N_1}{K} \\
p\gamma^\varphi & -k_5^\varphi & 0 & 0 \\
q\gamma^\varphi & \pi_2 \theta^\varphi & -k_6^\varphi & 0 \\
0 & \alpha_1^\varphi & \alpha_2^\varphi & -\tau^\varphi
\end{pmatrix}.$$

It is easy to verify that $\mathcal{J}_{11}$ has all its eigenvalues nonpositive. It thus remains to show that the ones of $\mathcal{J}_{22}$ are also nonpositive. The characteristic equation of $\mathcal{J}_{22}$ is given by

$\mathcal{P}(z) = a_1 z^4 + a_2 z^3 + a_3 z^2 + a_4 z + a_5 = 0$, where $a_1 = k_9^{\varphi} k_{10}^{\varphi}$, $a_2 = k_9^{\varphi} k_{10}^{\varphi} (\tau^{\varphi} + k_6^{\varphi} + k_5^{\varphi} + k_4^{\varphi})$,

$$
\begin{aligned}
a_3 &= k_{10}^{\varphi} \left[(k_6^{\varphi} + k_5^{\varphi} + k_4^{\varphi}) k_9^{\varphi} \tau^{\varphi} + k_5^{\varphi} k_6^{\varphi} k_9^{\varphi} + k_4^{\varphi} k_6^{\varphi} (p k_6^{\varphi} + \pi_2 p \theta^{\varphi} + k_5^{\varphi} q (1 - \mathcal{R}_h)) \right. \\
&\quad \left. + k_4^{\varphi} k_5^{\varphi} (k_8^{\varphi} + p k_6^{\varphi} (1 - \mathcal{R}_h)) \right], \\
a_4 &= k_4^{\varphi} k_5^{\varphi} k_6^{\varphi} k_{10}^{\varphi} \left[\mathcal{R}_h (\tau^{\varphi} + k_5^{\varphi} q) + k_6^{\varphi} p (\mathcal{R}_h + 1) + p \pi_2 \theta^{\varphi} (1 - \mathcal{R}_h) \right] \\
&\quad + k_4^{\varphi} k_5^{\varphi} k_6^{\varphi} k_9^{\varphi} \tau^{\varphi} (p \alpha_1^{\varphi} + \alpha_2^{\varphi} q) (1 - \mathcal{R}_e) + k_4^{\varphi} k_9^{\varphi} \tau^{\varphi} \left[\alpha_2^{\varphi} \pi_2 p \theta^{\varphi} (k_5^{\varphi} + k_6^{\varphi}) + (k_5^{\varphi})^2 \alpha_2^{\varphi} q + (k_6^{\varphi})^2 \alpha_1^{\varphi} p \right] \\
&\quad + k_5^{\varphi} k_6^{\varphi} k_9^{\varphi} k_{10}^{\varphi} \tau^{\varphi}, \\
a_5 &= k_4^{\varphi} k_5^{\varphi} k_6^{\varphi} \tau^{\varphi} (\pi_2 p \theta^{\varphi} + k_5^{\varphi} q + k_6^{\varphi} p) (\alpha_2^{\varphi} \pi_2 p \theta^{\varphi} + \alpha_2^{\varphi} k_5^{\varphi} q + \alpha_1^{\varphi} k_6^{\varphi} p) (1 - \mathcal{R}_c).
\end{aligned}
$$

Coefficients a_1, a_2 are always positive. Coefficient a_5 is positive (resp. negative) iff $\mathcal{R}_c < 1$ (resp. $\mathcal{R}_c > 1$). Since $\mathcal{R}_c < 1 \Longrightarrow (\mathcal{R}_h < 1 \ \& \ \mathcal{R}_e < 1)$, it follows that a_3 and a_4 are also positive. Then, $\mathcal{E}_0$ is locally asymptotically stable iff the following Routh-Hurwitz conditions hold

$$
\begin{aligned}
a_2 a_3 - a_4 &> 0, \\
a_2 (a_3 a_4 - a_2 a_5) - a_1 a_3^2 &> 0.
\end{aligned}
\tag{34}
$$

We thus claim what follows:

Lemma 7. *Assume that condition (34) holds. Then, the disease-free equilibrium of the fractional model (26) is locally asymptotically stable whenever $\mathcal{R}_c < 1$.*

From [3, Corollarly 2], we use the same Lyapunoy-type function to prove the global stability of the DFE for the classical model (13), we prove that the DFE of the fractional model (26) is globally asymptotically stable in Υ^{φ} whenever $\mathcal{R}_c < 1$. Thus, the following result is valid.

Theorem 8. *Assume that condition (34) holds. Then, the disease-free equilibrium of the fractional model (26) is globally asymptotically stable whenever $\mathcal{R}_c < 1$.*

4.2.3. Numerical scheme

To construct a numerical scheme of the fractional model (26), we used the Adams-type predictor-corrector iterative scheme [9, 10]. To this aim, let us consider the uniform discretization of $[0, a]$ given by $t_m = mh$, $m \in [0; N] \cap \mathbb{N}$ where $h = a/m$ denotes the step size. For a given approximation $x_h(t_i) \approx x(t_i)$, the next approximation $x_h(t_{i+1})$ is obtained (using the predictor-corrector method) as follows:

$$
\text{Predictor: } x_h^p(t_{n+1}) = \sum_{l=0}^{\lceil \varphi \rceil - 1} \frac{t_{n+1}^l}{l!} x_0^l + \frac{1}{\Gamma(\varphi)} \sum_{l=0}^{m} d_{l,m+1} \mathbb{K}(t_l, x_h(t_l));
$$

$$
\text{Corrector: } x_h(t_{n+1}) = \sum_{l=0}^{\lceil \varphi \rceil - 1} \frac{t_{n+1}^l}{l!} x_0^l + \frac{h^{\varphi}}{\Gamma(2+\varphi)} \mathbb{K}\left(t_{l+1}, x_h^h(t_{l+1})\right) + \frac{h^{\varphi}}{\Gamma(2+\varphi)} \sum_{l=0}^{m} b_{l,m+1} \mathbb{K}(t_l, x_h(t_l));
$$

with

$$
b_{l,m+1} = \begin{cases} m^{1+\varphi} - (m-\varphi)(m+1)^{\varphi}, & \text{if} \quad l = 0, \\ (m-l+2)^{1+\varphi} + (m-l)^{1+\varphi} - 2(m-l+1)^{1+\varphi}, & \text{if} \quad 1 \leq l \leq m, \\ 1 & \text{if} \quad l = m+1, \end{cases}
$$

and $d_{l,m+1} = \dfrac{h^{\varphi}}{\varphi} [(m-l+1)^{\varphi} - (m-l)^{\varphi}]$.

5. Numerical simulations and discussion

Here, we perform several numerical simulations to *(1)* Validate our theoretical results; and *(2)* compare the use of integer derivatives with fractional derivatives (which of the two permits to better predicting the disease spread in a short, medium or, long term).

5.1. General dynamics

Figure 9 illustrates the situation of the disease when the control reproduction number is greater that one. Indeed, when $\mathcal{R}_c > 1$ implies that the disease will persist in the population. Although we did not prove the uniqueness of the endemic equilibrium point as well as its global asymptotic stability, the figure 9 suggests that the model admits a globally asymptotically stable endemic equilibrium point whenever $\mathcal{R}_c$ is greater than 1.

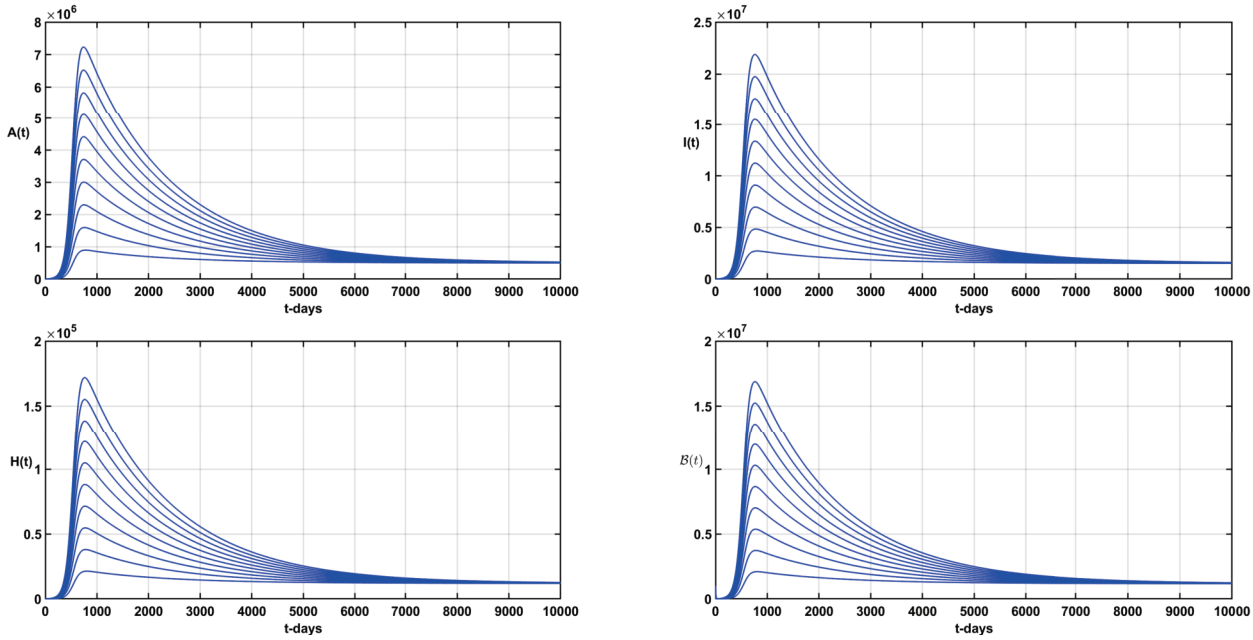

Figure 9: Time-series of $A(t)$, $I(t)$, $H(t)$ and $\mathcal{B}(t)$ with the above parameter values of Table 2. In this case $\mathcal{R}_c = 1.899451294774579 > 1$.

Figure 10 illustrate the result of Lemma 3 and Theorem 4. Indeed, if some other control measures like social distancing, wearing a mask continuously, and Confinement, are combined with vaccine and quarantine, the control reproduction number $\mathcal{R}_c$ should be less than one, then it is possible that, in long-term, the disease dies out.

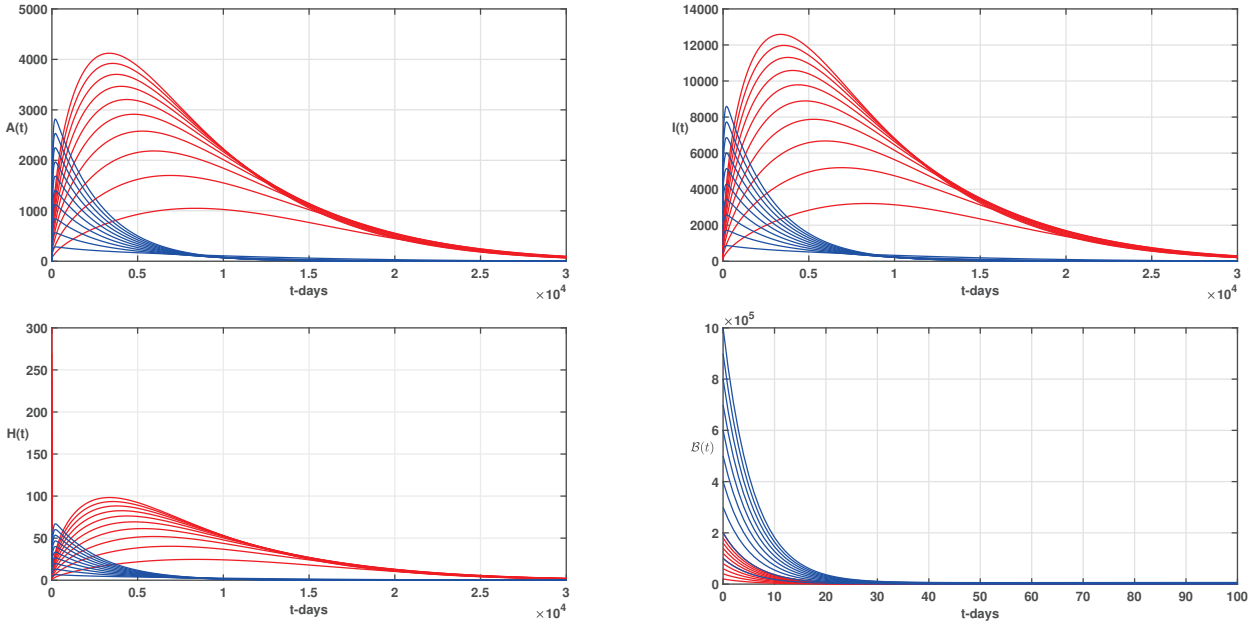

Figure 10: Time-series of $A(t)$, $I(t)$, $H(t)$ and $\mathcal{B}(t)$ with the above parameter values of Table 2 except $\beta_1 = 0.027$. In this case $\mathcal{R}_c = 0.9787 < 1$ and the disease will die out in the population.

5.2. Impact of the fractional operator

The impact of fractional derivative on the Covid-19 dynamics is depicted in Figures 11-12. Figure 11 depicts $\mathcal{R}_c$ as function of the fractional order φ. It is clear that $\mathcal{R}_c$ is an increasing function of φ. Indeed, $\varphi \in [0.5; 1]$ implies $\mathcal{R}_c \in [0.77; 1.8998]$ with $\mathcal{R}_c = 1$ when $\varphi \approx 0.681$. In a quantitative point of view, we note that the model with integer derivative ($\varphi = 1$) struggles to hug data on the long-term predictions. Indeed, in Figure 12, it is clear that it is only from $\varphi \approx 0.87$ that the fractional-order model better fits the data. Thus the model with fractional derivative (in the Caputo sense) is better than the model with integer derivative in the prediction of the Covid-19 new cases. From Figure 13, we see that using a model with classical derivatives (integer derivative) can overestimate the total number of news cases. Indeed, we see in Figure 13 that at $t \approx 744$ *days*, the epidemic peak is reached with $21,850,146$ cases for $\varphi = 1$, while for $\varphi = 0.84$, the epidemic peak is reached with $11,843,669$ cases at $t \approx 1224$ *days*.

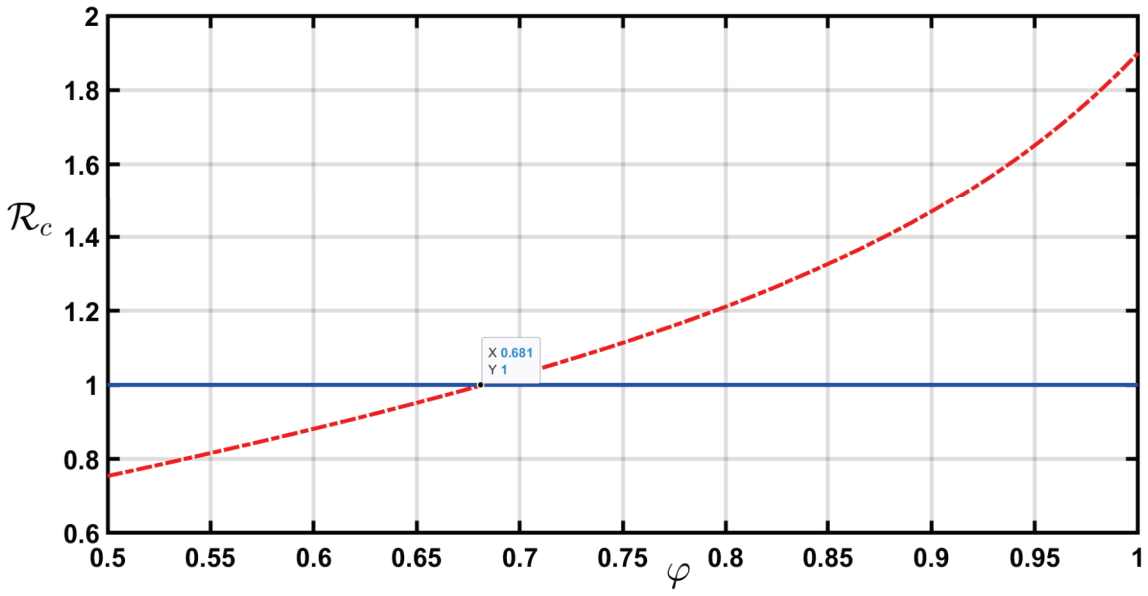

Figure 11: 2-D plot of $\mathcal{R}_c$ as a function of the fractional-order. The parameter values are those of Table 2.

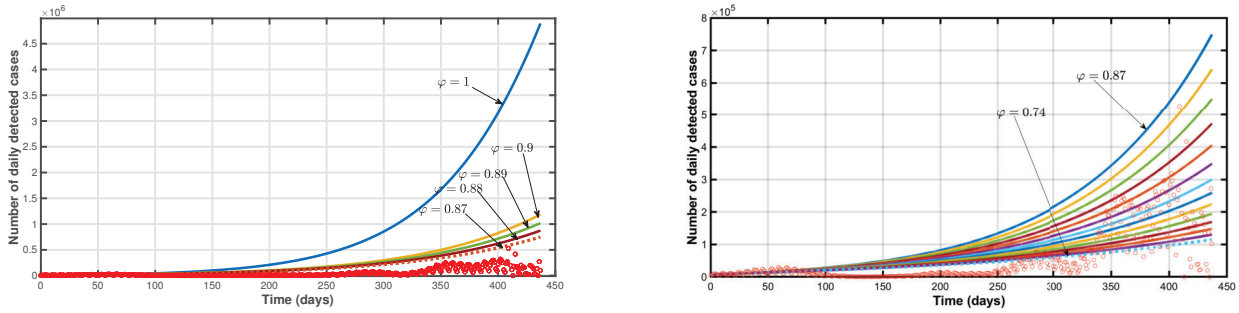

Figure 12: Long-term forecasting of Coronavirus (Covid-19) with varying the fractional-order parameter $\varphi \in [0.87; 1]$ (left panel) and $\varphi \in [0.74; 0.87]$ (right panel). The parameter values are those of Table 2. $t = 0$ stands for February 15, 2021 and $t = 437$ stands for April 28, 2022. We see that curves with fractional-order φ less than 0.87 better fit the data comprising the days between $t = 300$ and $t = 437$.

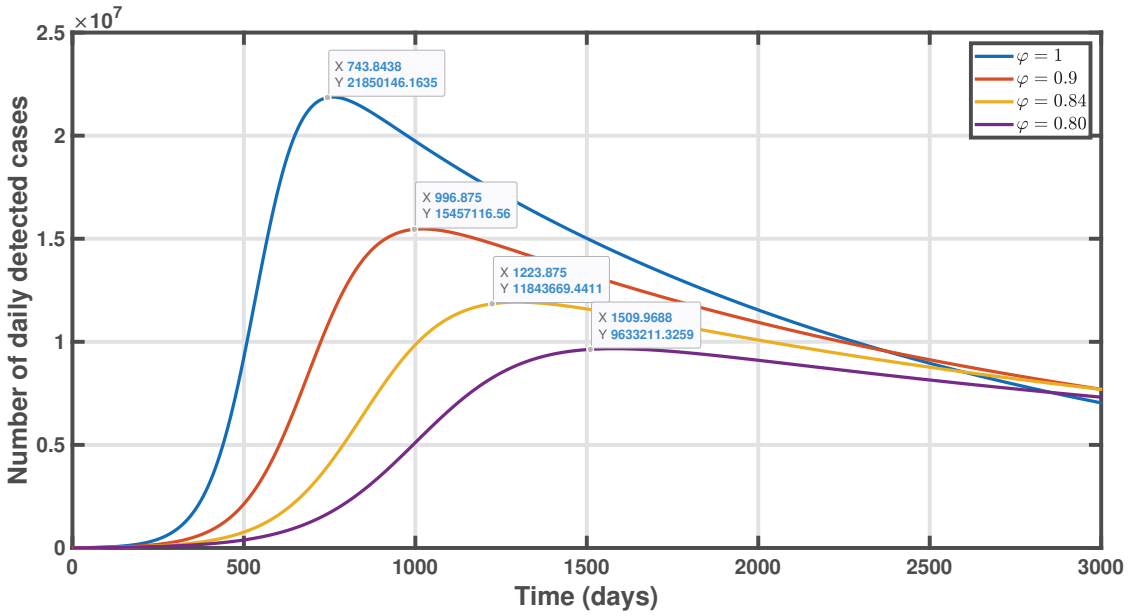

Figure 13: 2-D plot of $\mathcal{R}_c$ as a function of the fractional-order. The parameter values are those of Table 2.

Figure 14 and 15 illustrate Theorem 8. We see that when $\mathcal{R}_c < 1$, all trajectories vanish to zero, which means that the DFE of the fractional model is globally asymptotically stable (Figure 14), while they tend to their maximum values which represent the endemic equilibrium point (Figure 15.

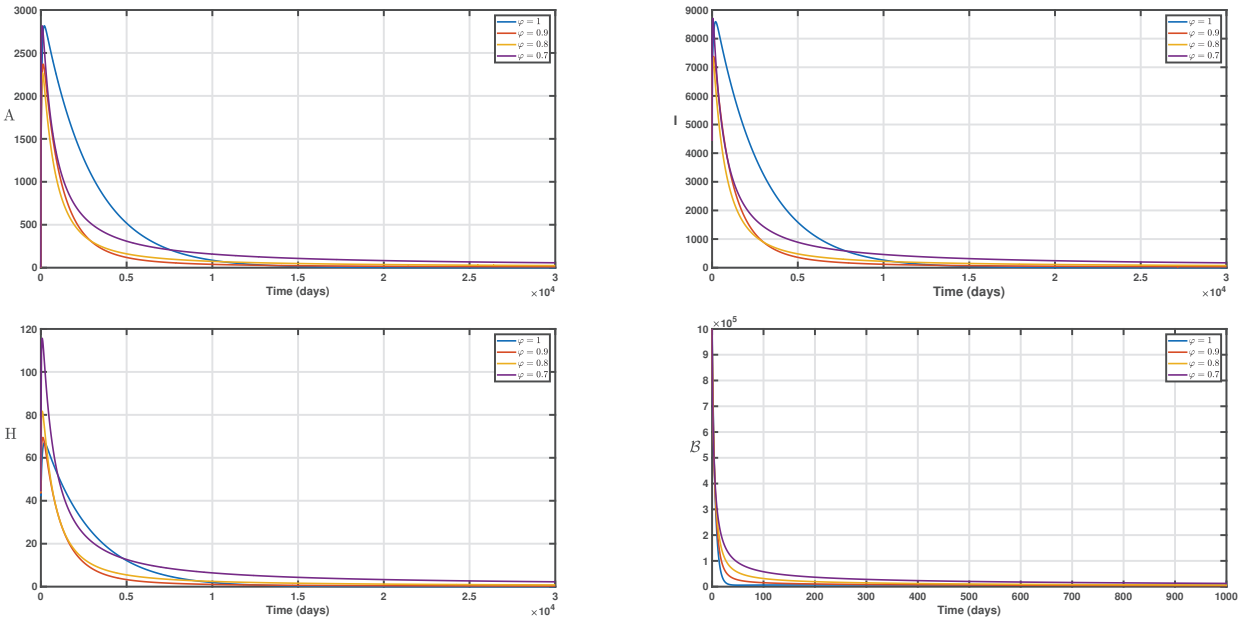

Figure 14: Time-series of $A(t)$, $I(t)$, $H(t)$ and $\mathcal{B}(t)$ with the parameter values listed in Table 2 except $\beta_1 = 0.027$ (to have $\mathcal{R}_c < 1$) for different values of the fractional order φ.

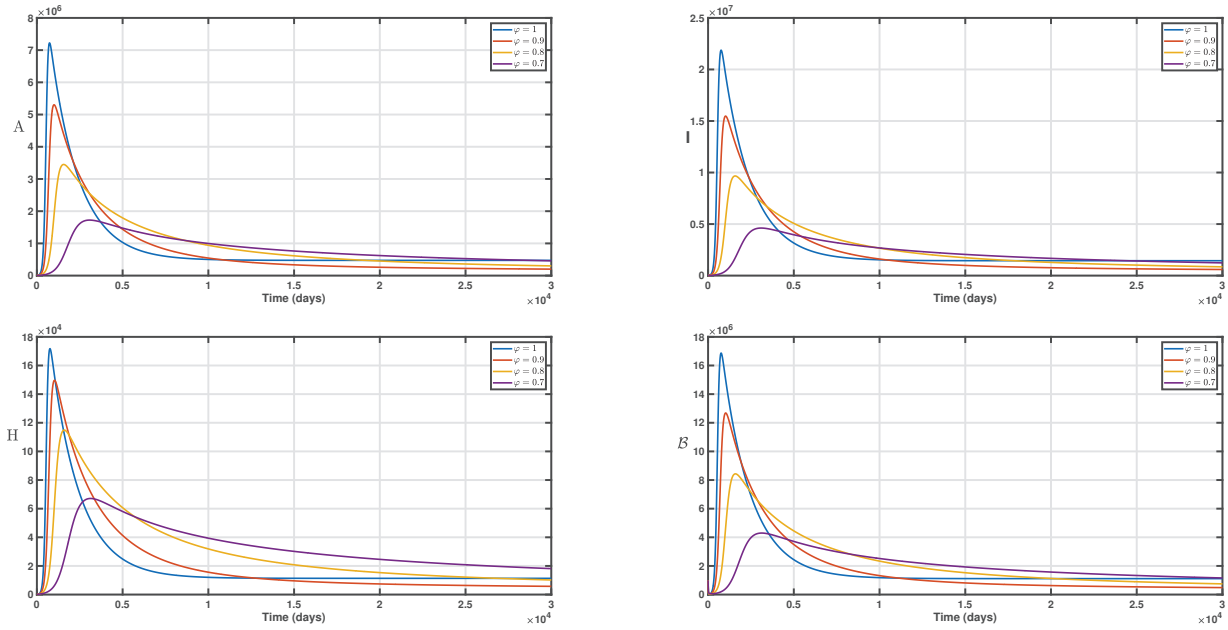

Figure 15: Time-series of $A(t)$, $I(t)$, $H(t)$ and $\mathcal{B}(t)$ with the parameter values listed in Table 2 for different values of the fractional order φ.

6. Conclusion and perspective

In this work, we formulated and analyzed a Covid-19 transmission dynamics model which takes into account two doses of the vaccination process, confinement, and treatment with limited resources, using both integer and fractional derivatives in the Caputo sense. After the model formulation with classical derivative, we started by establishing the positivity, boundedness, existence, and uniqueness of solutions. Then, we computed the control reproduction number $\mathcal{R}_c$ and perform the local and global asymptotic stability of the disease-free equilibrium whenever $\mathcal{R}_c < 1$. Indeed, we constructed a Lyapunov function and applied the comparison theorem to prove that the disease-free equilibrium is GAS whenever the control reproduction number is less than one. In the other words, this means that if existing controls can achieve that $\mathcal{R}_c < 1$, then the disease will die out. After that, we took the case $\mathcal{R}_c > 1$ and proved the existence of at less than one endemic equilibrium point. We then calibrate the model by estimating the model parameters with German data. With these estimated parameter values, we found that the control reproduction number is approximately equal to 1.90, which means that we are in endemic state since the control reproduction number is greater than one. Thus, intensification of control measures is needed to decrease this threshold under unity. We also found through numerical simulations that intensification of mass vaccination campaigns with a Covid-19 vaccine with a high efficacy level can permit to decrease the disease burden. We then performed global sensitivity analysis by computing partial rank correlation coefficients (PRCC) between $\mathcal{R}_c$ (respectively infected states) and each model parameters. We found that the most influential model parameters are β_1, γ, ϕ_2, θ, ν, η and ζ. This suggest that, control measures like individual protection, prevention and treatment (with high level of efficacy) combined with all measures which consist to detect new cases as well as which can boost the immunity system must be intensified to fight against the persistence of Covid-19 in the population.

After that, we formulated the corresponding fractional model in the Caputo sense. As

in the case of the integer model, we proved the positivity, boundedness, existence, and uniqueness of solutions. We also computed the control reproduction number of the fractional model, which depends on the fractional order φ. So, if the fractional order $\varphi = 1$, then both models have the same control reproduction number. Using the same approach as the case of the integer model, we proved the global asymptotic stability of the disease-free equilibrium whenever the control reproduction number is less than one, as well as the existence of an endemic equilibrium point whenever the control reproduction number is greater than one. We constructed a numerical scheme of the fractional number using the Adams-type predictor-corrector iterative method. To validate the theoretical analysis of both models, and compare the two types of derivatives, we performed several numerical simulations. We found that for a long-term prediction of new daily cases, the fractional model is better than the model with integer derivative. Indeed, when the fractional order φ is less than 0.87, the model with fractional derivative best fits the data in comparison to the model with classical derivatives. For both models, numerical simulations showed that all infected compartments go to zero whenever $\mathcal{R}_c < 1$, which confirms the GAS of the disease-free equilibrium. Although we did not prove the uniqueness of the endemic equilibrium, numerical simulations indicate that the model can have a unique endemic equilibrium that is globally asymptotically stable.

In the present work, we considered constant controls. It would be more realistic to replace constant controls with time-dependent controls. And thus, one should use the optimal control theory to make decisions like (1) the percentage of the population that should be vaccinated as the progression of the Covid-19 pandemic, to minimize the number of people infected, (2) the cost of implementing the vaccination strategy, and (3) which controls must be combined with vaccination to decrease rapidly the disease burden. This represents a direct perspective of this work.

Acknowledgment

The authors thank the Ministry of Science, Research and the Arts of the State of Baden-Württemberg (Ministerium für Wissenschaft, Forschung und Kunst Baden-Württemberg) for the grant supporting a joint research project within the 2022 initiative "Science Cooperation Africa (2021/2022)" which permitted the first author to have a research stay at the Department of Mathematics and Statistics of the University of Konstanz-Germany. The first author also thanks the Zukunftskolleg for providing him with all the necessary logistics during this research stay at the University of Konstanz.

Conflict of interest

The authors declare that they have no conflict of interest.

Appendix

A. Proof of Theorem 1

From (13), we have

$$\begin{cases} \dfrac{dS}{dt}(t)\Big|_{S=0,Q\geq 0} = r_2\Lambda + c_1Q(t) > 0, \quad \dfrac{dQ}{dt}(t)\Big|_{Q=0,S\geq 0} = r_1\Lambda + c_2S(t) > 0, \\ \dfrac{dV_1}{dt}(t)\Big|_{V_1=0,S\geq 0} = r_3\Lambda + v_1S(t) > 0, \quad \dfrac{dV_2}{dt}(t)\Big|_{V_{20}=0,V_1\geq 0} = \pi_1\Lambda + v_2V_1(t) > 0, \\ \dfrac{d\mathcal{B}}{dt}(t)\Big|_{\mathcal{B}=0,A,I\geq 0} = \alpha_1A(t) + \alpha_2I(t) \geq 0, \quad \dfrac{dA}{dt}(t)\Big|_{A=0,E\geq 0} = (1-q)\gamma E(t) \geq 0, \\ \dfrac{dI}{dt}(t)\Big|_{I=0,E,A\geq 0} = q\gamma E(t) + \pi_2\theta A(t) \geq 0, \quad \dfrac{dH}{dt}(t)\Big|_{H=0,A,I\geq 0} = \pi_3\nu I(t) + \psi_2\theta A(t) \geq 0, \\ \dfrac{dR}{dt}(t)\Big|_{R=0,A,I,H\geq 0} = \zeta H(t) + T(\sigma, H(t))(t) + \nu\eta I(t) + \psi_1\theta A(t) \geq 0, \\ \dfrac{dE}{dt}(t)\Big|_{E=0,S,Q,V_1,V_2,A,I,R,\mathcal{B}\geq 0} = \left(\beta_1\dfrac{A(t)+I(t)}{N(t)-H(t)} + \beta_2\dfrac{\mathcal{B}(t)}{K+\mathcal{B}(t)}\right) \\ \qquad \times (\phi_5R(t) + \phi_1Q(t) + \phi_2S(t) + \phi_3V_1(t) + \phi_4V_2(t)) \geq 0. \end{cases} \tag{35}$$

So, the nonnegativity of state variables of system (13) are obtained thanks to the Barrier theorem [20]. This means that $\mathbb{R}^{10}_+$ is an invariant set for the system (13).

B. Proof of Theorem 2

Adding the first nine equations of system (13) together, it follows that

$$\frac{dN}{dt}(t) := \sum_{i=1}^{9}\frac{d}{dt}x_i(t) = \Lambda - \mu\left(\sum_{i=1}^{9}x_i(t)\right) - \delta_1x_7 - \delta_2x_8 \leq \Lambda - \mu\left(\sum_{i=1}^{9}x_i(t)\right).$$

Solving this inequality gives

$$0 \leq N(t) := \sum_{i=1}^{9}x_i(t) \leq \frac{\Lambda}{\mu} + \left(\sum_{i=1}^{9}x_i(0) - \frac{\Lambda}{\mu}\right)e^{-\mu t}, \quad \text{for all } t \geq 0.$$

This implies, by passing to the limit, that $\limsup_{t\longrightarrow+\infty} N(t) \leq \dfrac{\Lambda}{\mu}$.

From the last equation of (13), we have

$$\frac{dx_{10}}{dt}(t) := \frac{d\mathcal{B}}{dt}(t) = \alpha_1x_6(t) + \alpha_2x_7(t) - \tau x_{10} \leq (\alpha_1+\alpha_2)\frac{\Lambda}{\mu} - \tau x_{10}.$$

Solving the above inequality gives

$$0 \leq x_{10}(t) = \mathcal{B}(t) \leq \frac{(\alpha_1+\alpha_2)\Lambda}{\mu\tau} + \left(x_{10}(0) - \frac{(\alpha_1+\alpha_2)\Lambda}{\mu\tau}\right)e^{-\tau t} \text{ for all } t \geq 0.$$

By passing to the limit, we obtain $\limsup_{t\longrightarrow+\infty} x_{10}(t) = \limsup_{t\longrightarrow+\infty} \mathcal{B}(t) \leq \dfrac{(\alpha_1+\alpha_2)\Lambda}{\mu\tau}$.

Thus, Υ is positively invariant and attracting for system (13).

C. Proof of Lemma 1

To prove Lemma (1), we just have to show that each $\dfrac{\partial \mathcal{F}_i}{\partial x_j}$, $1 \leq i, j \leq 10$ exists and is continuous. From (13) and using the fact that each state variable of system (13) is bounded, we have:

$$
\begin{array}{lll}
\dfrac{\partial \mathcal{F}_1}{\partial S} = -k_1 - \phi_2\lambda + \phi_2\beta_1 S\left[\dfrac{A+I}{(N-H)^2}\right], & \left|\dfrac{\partial \mathcal{F}_1}{\partial S}\right| \leq k_1 + \phi_2 + \phi_2\beta_1 < +\infty, \\
\dfrac{\partial \mathcal{F}_1}{\partial Q} = c_1 + \phi_2\beta_1\dfrac{(A+I)S}{(N-H)^2}, & \left|\dfrac{\partial \mathcal{F}_1}{\partial S}\right| \leq c_1 + \phi_2\beta_1 < +\infty, \\
\dfrac{\partial \mathcal{F}_1}{\partial V_1} = \phi_2\beta_1\dfrac{(A+I)S}{(N-H)^2}, & \left|\dfrac{\partial \mathcal{F}_1}{\partial V_1}\right| \leq \phi_2\beta_1 < +\infty, \\
\dfrac{\partial \mathcal{F}_1}{\partial V_2} = \phi_2\beta_1\dfrac{(A+I)S}{(N-H)^2}, & \left|\dfrac{\partial \mathcal{F}_1}{\partial V_2}\right| \leq \phi_2\beta_1 < +\infty, \\
\dfrac{\partial \mathcal{F}_1}{\partial E} = \phi_2\beta_1\dfrac{(A+I)S}{(N-H)^2}, & \left|\dfrac{\partial \mathcal{F}_1}{\partial E}\right| \leq \phi_2\beta_1 < +\infty, \\
\dfrac{\partial \mathcal{F}_1}{\partial A} = -\phi_2\beta_1\dfrac{(N-H-A-I)S}{(N-H)^2}, & \left|\dfrac{\partial \mathcal{F}_1}{\partial A}\right| \leq \phi_2\beta_1 < +\infty, \\
\dfrac{\partial \mathcal{F}_1}{\partial I} = -\phi_2\beta_1\dfrac{(N-H-A-I)S}{(N-H)^2}, & \left|\dfrac{\partial \mathcal{F}_1}{\partial I}\right| \leq \phi_2\beta_1 < +\infty, \\
\dfrac{\partial \mathcal{F}_1}{\partial H} = 0, & \left|\dfrac{\partial \mathcal{F}_1}{\partial H}\right| \leq +\infty, \\
\dfrac{\partial \mathcal{F}_1}{\partial R} = -\phi_2\beta_1\dfrac{(A+I)S}{(N-H)^2}, & \left|\dfrac{\partial \mathcal{F}_1}{\partial R}\right| \leq \phi_2\beta_1 < +\infty, \\
\dfrac{\partial \mathcal{F}_1}{\partial \mathcal{B}} = -\phi_2\beta_2\dfrac{K}{(K+B)^2}S, & \left|\dfrac{\partial \mathcal{F}_1}{\partial \mathcal{B}}\right| \leq \phi_2\beta_2\,|S| < +\infty,
\end{array}
\tag{36}
$$

We proceed by the similarly way for $\frac{\partial \mathcal{F}_j}{\partial x_i}$, $1 \leq i \leq 10$; $2 \leq j \leq 10$. Thus, we conclude that each $\frac{\partial \mathcal{F}_i}{\partial x_j}$, for $i, j \in [1, 10] \cap \mathbb{N}$, is continuous and bounded.

D. Proof of Proposition 1

To find stationary (equilibrium) points of system (13) for the special case, we set the right-hand side of (13) equal to zero. That is

$$
\left\{
\begin{array}{lll}
r_2\Lambda + c_1Q^\star - [k_1 + \phi_2\lambda^\star]\,S^\star &=& 0, \\
r_1\Lambda + c_2S^\star - [k_2 + \phi_1\lambda^\star]\,Q^\star &=& 0, \\
r_3\Lambda + v_1S^\star - [k_3 + \phi_3\lambda^\star]\,V_1^\star &=& 0, \\
\pi_1\Lambda + v_2V_1^\star - [\mu + \phi_4\lambda^\star]\,V_2^\star &=& 0, \\
\lambda^\star(\phi_5R^\star + \phi_1Q^\star + \phi_2S^\star + \phi_3V_1^\star + \phi_4V_2^\star) - k_4E^\star &=& 0, \\
p\gamma E^\star - k_5A^\star &=& 0, \\
q\gamma E^\star + \pi_2\theta A^\star - k_6I^\star &=& 0, \\
\pi_3\nu I^\star + \psi_2\theta A^\star - k_7H^\star &=& 0, \\
\zeta H^\star + \nu\eta I^\star + \psi_1\theta A^\star - [\mu + \phi_5\lambda^\star]\,R^\star &=& 0, \\
\alpha_1A^\star + \alpha_2I^\star - \tau\mathcal{B}^\star &=& 0,
\end{array}
\right.
\tag{37}
$$

where

$$\lambda^\star := \beta_1 \frac{A^\star + I^\star}{N^\star - H^\star} + \beta_2 \frac{\mathcal{B}^\star}{K + \mathcal{B}^\star}. \tag{38}$$

The resolution of the first seven equations coupled with the tenth equation of (37) in term of $\lambda^\star$ gives

$$\left\{ \begin{array}{rcl} S^\star & = & \dfrac{r_2\Lambda + c_1 Q^\star}{[k_1 + \phi_2\lambda^\star]}, Q^\star = \dfrac{r_1\Lambda + c_2 S^\star}{[k_2 + \phi_1\lambda^\star]}, V_1^\star = \dfrac{r_3\Lambda + v_1 S^\star}{[k_3 + \phi_3\lambda^\star]}, V_2^\star = \dfrac{\pi_1\Lambda + v_2 V_1^\star}{[\mu + \phi_4\lambda^\star]}, \\ E^\star & = & \dfrac{\lambda^\star(\phi_5 R^\star + \phi_1 Q^\star + \phi_2 S^\star + \phi_3 V_1^\star + \phi_4 V_2^\star)}{k_4}, A^\star = \dfrac{p\gamma E^\star}{k_5}, \\ I^\star & = & \dfrac{q\gamma E^\star + \pi_2\theta A^\star}{k_6}, \mathcal{B}^\star = \dfrac{\alpha_1 A^\star + \alpha_2 I^\star}{\tau} \end{array} \right. \tag{39}$$

Using (39) in the eighth equation of (37) gives

$$\begin{array}{l} \pi_3\nu I^\star + \psi_2\theta A^\star - k_7 H^\star = 0, \\ \Longleftrightarrow \left[\dfrac{\pi_3\nu\gamma}{k_6}\left(\dfrac{qk_5 + p\pi_2\theta}{k_5}\right) + \psi_2\theta\dfrac{p\gamma}{k_5}\right] E^\star - k_7 H^\star = 0, \\ \Longleftrightarrow \left[\dfrac{\pi_3\nu\gamma}{k_6}\left(\dfrac{qk_5 + p\pi_2\theta}{k_5}\right) + \psi_2\theta\dfrac{p\gamma}{k_5}\right] \dfrac{\lambda^\star\phi_5 R^\star}{k_4} \\ + \left[\dfrac{\pi_3\nu\gamma}{k_6}\left(\dfrac{qk_5 + p\pi_2\theta}{k_5}\right) + \psi_2\theta\dfrac{p\gamma}{k_5}\right] \dfrac{\lambda^\star(\phi_1 Q^\star + \phi_2 S^\star + \phi_3 V_1^\star + \phi_4 V_2^\star)}{k_4} - k_7 H^\star = 0, \end{array} \tag{40}$$

Solving the ninth equation of (37) gives

$$R^\star = \left\{\zeta H^\star + \frac{k_{11}}{k_4}\lambda^\star\left(\phi_1 Q^\star + \phi_2 S^\star + \phi_3 V_1^\star + \phi_4 V_2^\star\right)\right\}\left\{\frac{k_4}{[k_4(\mu + \phi_5\lambda^\star) - k_{11}\phi_5\lambda^\star]}\right\}, \tag{41}$$

where $k_{11} = \left[\frac{\nu\eta\gamma(qk_5 + p\pi_2\theta)}{k_5 k_6} + \frac{\psi_1\theta p\gamma}{k_5}\right]$.

Merging (41) in (40) gives

$$\frac{k_{12}\lambda^\star\phi_5}{k_4}\frac{1}{[\mu + \phi_5\lambda^\star]}\left\{\zeta H^\star + \frac{k_{11}}{k_4}\lambda^\star\mathcal{G}(\lambda^*)\right\}\left\{1 - \frac{k_{11}\phi_5\lambda^\star}{k_4[\mu + \phi_5\lambda^\star]}\right\}^{-1} + k_{12}\frac{\lambda^\star\mathcal{G}(\lambda^*)}{k_4} - k_7 H^\star = 0,$$

which gives

$$H^\star = \left\{\frac{k_{11}k_{12}\phi_5\lambda^\star + k_{12}[k_4(\mu + \phi_5\lambda^\star) - k_{11}\phi_5\lambda^\star]}{k_4 k_7[k_4(\mu + \phi_5\lambda^\star) - k_{11}\phi_5\lambda^\star] - k_4 k_{12}\phi_5\zeta\lambda^\star}\right\}\lambda^\star\mathcal{G}(\lambda^*), \tag{42}$$

where $k_{12} = \left[\frac{\pi_3\nu\gamma}{k_6}\left(\frac{qk_5 + p\pi_2\theta}{k_5}\right) + \psi_2\theta\frac{p\gamma}{k_5}\right]$ and $\mathcal{G}(\lambda^*) = \phi_1 Q^\star + \phi_2 S^\star + \phi_3 V_1^\star + \phi_4 V_2^\star$.

Using (39), (41) and (42) in (38), it follows that find the equilibrium points of model (13) in this special case consists in the resolution of the following equation

$$\mathcal{P}(\lambda^\star) := \lambda^\star\left[A_4(\lambda^\star)^4 + A_3(\lambda^\star)^3 + A_2(\lambda^\star)^2 + A_1\lambda^\star + A_0\right] = 0 \tag{43}$$

where

$$A_0 = -k_4^2 k_5^2 k_6^2 k_7^2 K\mu^4\tau\left(\mathcal{R}_c - 1\right),$$

$$
\begin{aligned}
A_4 &= \phi_5^2 k_7 \times ... \\
&\times \left(p\theta\gamma\left[\pi_2\left(\nu+\delta_1\right)+k_6\left(\psi_2+\psi_1\right)\right]+k_5 q\gamma\left(\nu+\delta_1\right)-k_4k_5k_6\right)\times ... \\
&\times \left(K\tau\gamma\zeta\left(\pi_3\nu\left(\theta\pi_2 p+k_5 q\right)+\psi_2 p k_6\theta\right)+k_7K\tau\gamma\left(\eta\nu\left(\pi_2 p\theta+k_5 q\right)+\psi_1 k_6 p\theta\right)\right. \\
&\left.-k_7\Lambda\gamma\left[\alpha_2\left(\pi_2 p\theta+k_5 q\right)+\alpha_1 k_6 p\right]-k_4k_5k_6k_7K\tau\right) \\
&= \phi_5^2 k_7 \times ... \\
&\times k_4k_5k_6\left(\frac{\gamma\left(\nu+\delta_1\right)k_8}{k_4k_5k_6}+\frac{p\theta\gamma\left(\psi_2+\psi_1\right)}{k_4k_5}-1\right)\times ... \\
&\times \left(K\tau\gamma\zeta\pi_3k_8\nu+K\tau\gamma k_7\psi_1k_6p\theta+K\tau\gamma\zeta\psi_2pk_6\theta+K\tau\gamma k_7\eta\nu k_8-k_7\Lambda\gamma k_{10}-k_4k_5k_6k_7K\tau\right),
\end{aligned}
$$

$$
\begin{aligned}
A_1 = {} & (((\beta_1\pi_2k_5\phi_5k_6k_7k_{12}K\mu^3p\tau+(\alpha_2\beta_2\pi_2k_5\phi_5-\alpha_2\beta_2\pi_2k_5)k_6k_7k_{12}\Lambda\mu^2p)\theta \\
&+(\beta_1k_5^2\phi_5k_6k_7k_{12}K\mu^3q+\beta_1k_5\phi_5k_6^2k_7k_{12}K\mu^3p)\tau+(\alpha_2\beta_2k_5^2\phi_5-\alpha_2\beta_2k_5^2)k_6k_7k_{12}\Lambda\mu^2q \\
&+(\alpha_1\beta_2k_5\phi_5-\alpha_1\beta_2k_5)k_6^2k_7k_{12}\Lambda\mu^2p)\gamma+(k_4k_5^2-2k_4k_5^2\phi_5)k_6^2k_7k_{12}K\mu^3\tau)\zeta \\
&+((\alpha_2\beta_2\pi_2^2\pi_3k_7^2\Lambda\mu^2\nu-\beta_1\alpha_2\pi_2^2k_7^2\Lambda\mu^3+(\alpha_2\beta_2\pi_2\psi_2k_6+\delta_1\alpha_2\beta_2\pi_2^2)k_7^2\Lambda\mu^2)p^2\theta^2 \\
&+((2\alpha_2\beta_2\pi_2\pi_3k_5k_7^2\Lambda\mu^2\nu-2\beta_1\alpha_2\pi_2k_5k_7^2\Lambda\mu^3+(\alpha_2b_2\psi_2k_5k_6+2\delta_1\alpha_2\beta_2\pi_2k_5)k_7^2\Lambda\mu^2)pq \\
&+(\alpha_1\beta_2\pi_2\pi_3k_6k_7^2\Lambda\mu^2\nu+(-\beta_1\alpha_2-\alpha_1\beta_1)\pi_2k_6k_7^2\Lambda\mu^3+(\alpha_1\beta_2\psi_2k_6^2+\alpha_1\delta_1\beta_2\pi_2k_6)k_7^2\Lambda\mu^2)p^2)\theta \\
&+(\alpha_2\beta_2\pi_3k_5^2k_7^2\Lambda\mu^2\nu-\beta_1\alpha_2k_5^2k_7^2\Lambda\mu^3+\delta_1\alpha_2\beta_2k_5^2k_7^2\Lambda\mu^2)q^2 \\
&+(\alpha_1\beta_2\pi_3k_5k_6k_7^2\Lambda\mu^2\nu+(-\beta_1\alpha_2-\alpha_1\beta_1)k_5k_6k_7^2\Lambda\mu^3+\alpha_1\delta_1\beta_2k_5k_6k_7^2\Lambda\mu^2)pq-\alpha_1\beta_1k_6^2k_7^2\Lambda\mu^3p^2)\gamma^2 \\
&+((((\beta_1\pi_2k_5\phi_5k_6k_7^2k_{11}+(((-\delta_1-\beta_1)\pi_2k_4k_5-2\beta_1\pi_2k_4k_5\phi_5)k_6-\psi_2k_4k_5k_6^2)k_7^2)K\mu^3-\pi_2\pi_3k_4k_5k_6k_7^2K\mu^3\nu)p\tau \\
&+(\alpha_2\pi_2k_4k_5k_6k_7^2\Lambda\mu^3+(\alpha_2\beta_2\pi_2k_5\phi_5k_6k_7^2k_{11}+(-2\alpha_2\beta_2\pi_2k_4k_5\phi_5-\alpha_2\beta_2\pi_2k_4k_5)k_6k_7^2)\Lambda\mu^2)p)\theta \\
&+(((\beta_1k_5^2\phi_5k_6k_7^2k_{11}+((-\delta_1-\beta_1)k_4k_5^2-2\beta_1k_4k_5^2\phi_5)k_6k_7^2)K\mu^3-\pi_3k_4k_5^2k_6k_7^2K\mu^3\nu)q \\
&+(\beta_1k_5\phi_5k_6^2k_7^2k_{11}+(-2\beta_1k_4k_5\phi_5-\beta_1k_4k_5)k_6^2k_7^2)K\mu^3p)\tau \\
&+(\alpha_2k_4k_5^2k_6k_7^2\Lambda\mu^3+(\alpha_2\beta_2k_5^2\phi_5k_6k_7^2k_{11}+(-2\alpha_2\beta_2k_4k_5^2\phi_5-\alpha_2\beta_2k_4k_5^2)k_6k_7^2)\Lambda\mu^2)q \\
&+(\alpha_1k_4k_5k_6^2k_7^2\Lambda\mu^3+(\alpha_1\beta_2k_5\phi_5k_6^2k_7^2k_{11}+(-2\alpha_1\beta_2k_4k_5\phi_5-\alpha_1\beta_2k_4k_5)k_6^2k_7^2)\Lambda\mu^2)p)\gamma \\
&+((2k_4^2k_5^2\phi_5+2k_4^2k_5^2)k_6^2k_7^2-2k_4k_5^2\phi_5k_6^2k_7^2k_{11})K\mu^3\tau,
\end{aligned}
$$

$$
\begin{aligned}
A_2 = {} & (k_5^2\phi_5^2 - k_5^2\phi_5)k_6^2k_{12}^2K\mu^2\tau\zeta^2 \\
& + ((((\pi_2\pi_3k_5\phi_5k_6k_7k_{12}K\mu^2\nu + (\psi_2k_5\phi_5k_6^2 + (b_1\pi_2k_5\phi_5^2 + (\delta_1+b_1)\pi_2k_5\phi_5)k_6)k_7k_{12}K\mu^2)p\tau \\
& + ((\alpha_2\pi_2k_5 - \alpha_2\pi_2k_5\phi_5)k_6k_7k_{12}\Lambda\mu^2 + (\alpha_2b_2\pi_2k_5\phi_5^2 - \alpha_2b_2\pi_2k_5\phi_5)k_6k_7k_{12}\Lambda\mu)p)\theta \\
& + ((\pi_3k_5^2\phi_5k_6k_7k_{12}K\mu^2\nu + (b_1k_5^2\phi_5^2 + (\delta_1+b_1)k_5^2\phi_5)k_6k_7k_{12}K\mu^2)q + (b_1k_5\phi_5^2 + b_1k_5\phi_5)k_6^2k_7k_{12}K\mu^2p)\tau \\
& + ((\alpha_2k_5^2 - \alpha_2k_5^2\phi_5)k_6k_7k_{12}\Lambda\mu^2 + (\alpha_2b_2k_5^2\phi_5^2 - \alpha_2b_2k_5^2\phi_5)k_6k_7k_{12}\Lambda\mu)q + ((\alpha_1k_5 - \alpha_1k_5\phi_5)k_6^2k_7k_{12}\Lambda\mu^2 \\
& + (\alpha_1b_2k_5\phi_5^2 - \alpha_1b_2k_5\phi_5)k_6^2k_7k_{12}\Lambda\mu)p)\gamma + ((2k_5^2\phi_5^2 - k_5^2\phi_5)k_6^2k_7k_{11} \\
& + (-2k_4k_5^2\phi_5^2 - 2k_4k_5^2\phi_5 + k_4k_5^2)k_6^2k_7)k_{12}K\mu^2\tau)\zeta + (((2\alpha_2b_2\pi_2^2\pi_3\phi_5k_7^2\Lambda\mu - \alpha_2\pi_2^2\pi_3k_7^2\Lambda\mu^2)\nu \\
& + (-\alpha_2\pi_2\psi_2k_6 - 2b_1\alpha_2\pi_2^2\phi_5 - \delta_1\alpha_2\pi_2^2)k_7^2\Lambda\mu^2 + (2\alpha_2b_2\pi_2\psi_2\phi_5k_6 + 2\delta_1\alpha_2b_2\pi_2^2\phi_5)k_7^2\Lambda\mu)p^2\theta^2 \\
& + (((4\alpha_2b_2\pi_2\pi_3k_5\phi_5k_7^2\Lambda\mu - 2\alpha_2\pi_2\pi_3k_5k_7^2\Lambda\mu^2)\nu + (-\alpha_2\psi_2k_5k_6 - 4b_1\alpha_2\pi_2k_5\phi_5 - 2\delta_1\alpha_2\pi_2k_5)k_7^2\Lambda\mu^2 \\
& + (2\alpha_2b_2\psi_2k_5\phi_5k_6 + 4\delta_1\alpha_2b_2\pi_2k_5\phi_5)k_7^2\Lambda\mu)pq + ((2\alpha_1b_2\pi_2\pi_3\phi_5k_6k_7^2\Lambda\mu - \alpha_1\pi_2\pi_3k_6k_7^2\Lambda\mu^2)\nu \\
& + (((-2b_1\alpha_2 - 2\alpha_1b_1)\pi_2\phi_5 - \alpha_1\delta_1\pi_2)k_6 - \alpha_1\psi_2k_6^2)k_7^2\Lambda\mu^2 + (2\alpha_1b_2\psi_2\phi_5k_6^2 + 2\alpha_1\delta_1b_2\pi_2\phi_5k_6)k_7^2\Lambda\mu)p^2)\theta \\
& + ((2\alpha_2b_2\pi_3k_5^2\phi_5k_7^2\Lambda\mu - \alpha_2\pi_3k_5^2k_7^2\Lambda\mu^2)\nu + (-2b_1\alpha_2k_5^2\phi_5 - \delta_1\alpha_2k_5^2)k_7^2\Lambda\mu^2 + 2\delta_1\alpha_2b_2k_5^2\phi_5k_7^2\Lambda\mu)q^2 \\
& + ((2\alpha_1b_2\pi_3k_5\phi_5k_6k_7^2\Lambda\mu - \alpha_1\pi_3k_5k_6k_7^2\Lambda\mu^2)\nu \\
& + ((-2b_1\alpha_2 - 2\alpha_1b_1)k_5\phi_5 - \alpha_1\delta_1k_5)k_6k_7^2\Lambda\mu^2 + 2\alpha_1\delta_1b_2k_5\phi_5k_6k_7^2\Lambda\mu)pq - 2\alpha_1b_1\phi_5k_6^2k_7^2\Lambda\mu^2p^2)\gamma^2 \\
& + ((((\pi_2\pi_3k_5\phi_5k_6k_7^2k_{11} + (-2\pi_2\pi_3k_4k_5\phi_5 - \pi_2\pi_3k_4k_5)k_6k_7^2)K\mu^2\nu \\
& + ((\psi_2k_5\phi_5k_6^2 + (b_1\pi_2k_5\phi_5^2 + (\delta_1+b_1)\pi_2k_5\phi_5)k_6)k_7^2k_{11} + ((-2\psi_2k_4k_5\phi_5 - \psi_2k_4k_5)k_6^2 \\
& + (-b_1\pi_2k_4k_5\phi_5^2 + (-2\delta_1 - 2b_1)\pi_2k_4k_5\phi_5 - \delta_1\pi_2k_4k_5)k_6)k_7^2)K\mu^2)p\tau \\
& + (((2\alpha_2\pi_2k_4k_5\phi_5 + \alpha_2\pi_2k_4k_5)k_6k_7^2 - \alpha_2\pi_2k_5\phi_5k_6k_7^2k_{11})\Lambda\mu^2 \\
& + ((\alpha_2b_2\pi_2k_5\phi_5^2 + \alpha_2b_2\pi_2k_5\phi_5)k_6k_7^2k_{11} + (-\alpha_2b_2\pi_2k_4k_5\phi_5^2 - 2\alpha_2b_2\pi_2k_4k_5\phi_5)k_6k_7^2)\Lambda\mu)p)\theta \\
& + (((\pi_3k_5^2\phi_5k_6k_7^2k_{11} + (-2\pi_3k_4k_5^2\phi_5 - \pi_3k_4k_5^2)k_6k_7^2)K\mu^2\nu + ((b_1k_5^2\phi_5^2 + (\delta_1+b_1)k_5^2\phi_5)k_6k_7^2k_{11} \\
& + (-b_1k_4k_5^2\phi_5^2 + (-2\delta_1 - 2b_1)k_4k_5^2\phi_5 - \delta_1k_4k_5^2)k_6k_7^2)K\mu^2)q + ((b_1k_5\phi_5^2 + b_1k_5\phi_5)k_6^2k_7^2k_{11} \\
& + (-b_1k_4k_5\phi_5^2 - 2b_1k_4k_5\phi_5)k_6^2k_7^2)K\mu^2p)\tau + (((2\alpha_2k_4k_5^2\phi_5 + \alpha_2k_4k_5^2)k_6k_7^2 - \alpha_2k_5^2\phi_5k_6k_7^2k_{11})\Lambda\mu^2 \\
& + ((\alpha_2b_2k_5^2\phi_5^2 + \alpha_2b_2k_5^2\phi_5)k_6k_7^2k_{11} + (-\alpha_2b_2k_4k_5^2\phi_5^2 - 2\alpha_2b_2k_4k_5^2\phi_5)k_6k_7^2)\Lambda\mu)q \\
& + (((2\alpha_1k_4k_5\phi_5 + \alpha_1k_4k_5)k_6^2k_7^2 - \alpha_1k_5\phi_5k_6^2k_7^2k_{11})\Lambda\mu^2 + ((\alpha_1b_2k_5\phi_5^2 + \alpha_1b_2k_5\phi_5)k_6^2k_7^2k_{11} \\
& + (-\alpha_1b_2k_4k_5\phi_5^2 - 2\alpha_1b_2k_4k_5\phi_5)k_6^2k_7^2)\Lambda\mu)p)\gamma + (k_5^2\phi_5^2k_6^2k_7^2k_{11}^2 + (-2k_4k_5^2\phi_5^2 - 4k_4k_5^2\phi_5)k_6^2k_7^2k_{11} \\
& + (k_4^2k_5^2\phi_5^2 + 4k_4^2k_5^2\phi_5 + k_4^2k_5^2)k_6^2k_7^2)K\mu^2\tau,
\end{aligned}
$$

$$
\begin{aligned}
A_3 &= (k_5^2\phi_5^2 - k_5^2\phi_5)k_6^2k_{12}^2K\mu\tau\zeta^2 + (((((\pi_2\pi_3k_5\phi_5^2 + \pi_2\pi_3k_5\phi_5)k_6k_7k_{12}K\mu\nu + ((\psi_2k_5\phi_5^2 + \psi_2k_5\phi_5)k_6^2 \\
&+ ((\delta_1+\beta_1)\pi_2k_5\phi_5^2 + \delta_1\pi_2k_5\phi_5)k_6)k_7k_{12}K\mu)p\tau + (\alpha_2\pi_2k_5\phi_5 - \alpha_2\pi_2k_5\phi_5^2)k_6k_7k_{12}\Lambda\mu p)\theta \\
&+ (((\pi_3k_5^2\phi_5^2 + \pi_3k_5^2\phi_5)k_6k_7k_{12}K\mu\nu + ((\delta_1+b_1)k_5^2\phi_5^2 + \delta_1k_5^2\phi_5)k_6k_7k_{12}K\mu)q + \beta_1k_5\phi_5^2k_6^2k_7k_{12}K\mu p)\tau \\
&+ (\alpha_2k_5^2\phi_5 - \alpha_2k_5^2\phi_5^2)k_6k_7k_{12}\Lambda\mu q + (\alpha_1k_5\phi_5 - \alpha_1k_5\phi_5^2)k_6^2k_7k_{12}\Lambda\mu p)\gamma \\
&+ ((3k_5^2\phi_5^2 - k_5^2\phi_5)k_6^2k_7k_{11} - 3k_4k_5^2\phi_5^2k_6^2k_7)k_{12}K\mu\tau)\zeta + (((\alpha_2\beta_2\pi_2^2\pi_3\phi_5^2k_7^2\Lambda - 2\alpha_2\pi_2^2\pi_3\phi_5k_7^2\Lambda\mu)\nu \\
&+ (-2\alpha_2\pi_2\psi_2\phi_5k_6 - \beta_1\alpha_2\pi_2^2\phi_5^2 - 2\delta_1\alpha_2\pi_2^2\phi_5)k_7^2\Lambda\mu + (\alpha_2\beta_2\pi_2\psi_2\phi_5^2k_6 + \delta_1\alpha_2\beta_2\pi_2^2\phi_5^2)k_7^2\Lambda)p^2\theta^2 \\
&+ (((2\alpha_2\beta_2\pi_2\pi_3k_5\phi_5^2k_7^2\Lambda - 4\alpha_2\pi_2\pi_3k_5\phi_5k_7^2\Lambda\mu)\nu + (-2\alpha_2\psi_2k_5\phi_5k_6 - 2\beta_1\alpha_2\pi_2k_5\phi_5^2 - 4\delta_1\alpha_2\pi_2k_5\phi_5)k_7^2\Lambda\mu \\
&+ (\alpha_2\beta_2\psi_2k_5\phi_5^2k_6 + 2\delta_1\alpha_2\beta_2\pi_2k_5\phi_5^2)k_7^2\Lambda)pq + ((\alpha_1\beta_2\pi_2\pi_3\phi_5^2k_6k_7^2\Lambda - 2\alpha_1\pi_2\pi_3\phi_5k_6k_7^2\Lambda\mu)\nu \\
&+ (((-\beta_1\alpha_2 - \alpha_1\beta_1)\pi_2\phi_5^2 - 2\alpha_1\delta_1\pi_2\phi_5)k_6 - 2\alpha_1\psi_2\phi_5k_6^2)k_7^2\Lambda\mu + (\alpha_1\beta_2\psi_2\phi_5^2k_6^2 + \alpha_1\delta_1\beta_2\pi_2\phi_5^2k_6)k_7^2\Lambda)p^2)\theta \\
&+ ((\alpha_2\beta_2\pi_3k_5^2\phi_5^2k_7^2\Lambda - 2\alpha_2\pi_3k_5^2\phi_5k_7^2\Lambda\mu)\nu + (-\beta_1\alpha_2k_5^2\phi_5^2 - 2\delta_1\alpha_2k_5^2\phi_5)k_7^2\Lambda\mu + \delta_1\alpha_2\beta_2k_5^2\phi_5^2k_7^2\Lambda)q^2 \\
&+ ((\alpha_1\beta_2\pi_3k_5\phi_5^2k_6k_7^2\Lambda - 2\alpha_1\pi_3k_5\phi_5k_6k_7^2\Lambda\mu)\nu \\
&+ ((-\beta_1\alpha_2 - \alpha_1\beta_1)k_5\phi_5^2 - 2\alpha_1\delta_1k_5\phi_5)k_6k_7^2\Lambda\mu + \alpha_1\delta_1\beta_2k_5\phi_5^2k_6k_7^2\Lambda)pq - \alpha_1b_1\phi_5^2k_6^2k_7^2\Lambda\mu p^2)\gamma^2 \\
&+ (((((\pi_2\pi_3k_5\phi_5^2 + \pi_2\pi_3k_5\phi_5)k_6k_7^2k_{11} + (-\pi_2\pi_3k_4k_5\phi_5^2 - 2\pi_2\pi_3k_4k_5\phi_5)k_6k_7^2)K\mu\nu \\
&+ (((\psi_2k_5\phi_5^2 + \psi_2k_5\phi_5)k_6^2 + ((\delta_1+\beta_1)\pi_2k_5\phi_5^2 + \delta_1\pi_2k_5\phi_5)k_6)k_7^2k_{11} + ((-\psi_2k_4k_5\phi_5^2 - 2\psi_2k_4k_5\phi_5)k_6^2 \\
&+ ((-\delta_1-\beta_1)\pi_2k_4k_5\phi_5^2 - 2\delta_1\pi_2k_4k_5\phi_5)k_6)k_7^2)K\mu)p\tau \\
&+ (((-\alpha_2\pi_2k_5\phi_5^2 - \alpha_2\pi_2k_5\phi_5)k_6k_7^2k_{11} + (\alpha_2\pi_2k_4k_5\phi_5^2 + 2\alpha_2\pi_2k_4k_5\phi_5)k_6k_7^2)\Lambda\mu \\
&+ (\alpha_2\beta_2\pi_2k_5\phi_5^2k_6k_7^2k_{11} - \alpha_2\beta_2\pi_2k_4k_5\phi_5^2k_6k_7^2)\Lambda)p)\theta \\
&+ ((((\pi_3k_5^2\phi_5^2 + \pi_3k_5^2\phi_5)k_6k_7^2k_{11} + (-\pi_3k_4k_5^2\phi_5^2 - 2\pi_3k_4k_5^2\phi_5)k_6k_7^2)K\mu\nu \\
&+ (((\delta_1+\beta_1)k_5^2\phi_5^2 + \delta_1k_5^2\phi_5)k_6k_7^2k_{11} + ((-\delta_1-\beta_1)k_4k_5^2\phi_5^2 - 2\delta_1k_4k_5^2\phi_5)k_6k_7^2)K\mu)q \\
&+ (\beta_1k_5\phi_5^2k_6^2k_7^2k_{11} - \beta_1k_4k_5\phi_5^2k_6^2k_7^2)K\mu p)\tau + (((-\alpha_2k_5^2\phi_5^2 - \alpha_2k_5^2\phi_5)k_6k_7^2k_{11} + (\alpha_2k_4k_5^2\phi_5^2 + 2\alpha_2k_4k_5^2\phi_5)k_6k_7^2)\Lambda\mu \\
&+ (\alpha_2\beta_2k_5^2\phi_5^2k_6k_7^2k_{11} - \alpha_2\beta_2k_4k_5^2\phi_5^2k_6k_7^2)\Lambda)q + (((-\alpha_1k_5\phi_5^2 - \alpha_1k_5\phi_5)k_6^2k_7^2k_{11} + (\alpha_1k_4k_5\phi_5^2 + 2\alpha_1k_4k_5\phi_5)k_6^2k_7^2)\Lambda\mu \\
&+ (\alpha_1\beta_2k_5\phi_5^2k_6^2k_7^2k_{11} - \alpha_1\beta_2k_4k_5\phi_5^2k_6^2k_7^2)\Lambda)p)\gamma \\
&+ (2k_5^2\phi_5^2k_6^2k_7^2k_{11}^2 + (-4k_4k_5^2\phi_5^2 - 2k_4k_5^2\phi_5)k_6^2k_7^2k_{11} + (2k_4^2k_5^2\phi_5^2 + 2k_4^2k_5^2\phi_5)k_6^2k_7^2)K\mu\tau.
\end{aligned}
$$

Coefficient A_0 is negative (resp. positive) if and only if $\mathcal{R}_c > 1$ (resp. $\mathcal{R}_c < 1$). The sign of the remaining coefficients depend of the parameters values. The proof is completed thanks to Descartes' rule of signs.

E. Proof of Theorem 6

Adding the first nine equations of system (26) together, it follows that

$$
{}_a^C\mathcal{D}_t^{\varphi}N(t) := \sum_{i=1}^{9} {}_0^C\mathcal{D}_t^{\varphi}x_i(t) = \Lambda^{\varphi} - \mu^{\varphi}\left(\sum_{i=1}^{9}x_i(t)\right) - \delta_1^{\varphi}x_7 - \delta_2^{\varphi}x_8 \leq \Lambda^{\varphi} - \mu^{\varphi}\left(\sum_{i=1}^{9}x_i(t)\right).
$$

Using the Mittag-Leffler function defined at Eq. (25) (see Definition 25), we obtain by solving the above inequality, that

$$
0 \leq N(t) := \sum_{i=1}^{9}x_i(t) \leq \frac{\Lambda^{\varphi}}{\mu^{\varphi}} + \left(\sum_{i=1}^{9}x_i(0) - \frac{\Lambda^{\varphi}}{\mu^{\varphi}}\right)\mathbf{E}_{\varphi}\left(-\mu^{\varphi}t\right), \quad \text{for all } t \geq 0.
$$

This implies, by passing to the limit, that $\limsup_{t\longrightarrow+\infty} N(t) \leq \dfrac{\Lambda^{\varphi}}{\mu^{\varphi}}$.

From the last equation of (13), we have

$$
{}_a^C\mathcal{D}_t^{\varphi}x_{10}(t) :=_0^C \mathcal{D}_t^{\varphi}\mathcal{B}(t) = \alpha_1^{\varphi}x_7(t) + \alpha_2^{\varphi}x_8(t) - \tau^{\varphi}x_{10} \leq (\alpha_1^{\varphi} + \alpha_2^{\varphi})\frac{\Lambda^{\varphi}}{\mu^{\varphi}} - \tau^{\varphi}x_{10}.
$$

Solving the above inequality gives

$$0 \leq x_{10}(t) = \mathcal{B}(t) \leq \frac{(\alpha_1^{\varphi} + \alpha_2^{\varphi})\Lambda^{\varphi}}{\mu^{\varphi}\tau^{\varphi}} + \left(x_{10}(0) - \frac{(\alpha_1^{\varphi} + \alpha_2^{\varphi})\Lambda^{\varphi}}{\mu^{\varphi}\tau^{\varphi}} \right) \mathbf{E}_{\varphi}\left(-\tau^{\varphi} t\right) \text{ for all } t \geq 0.$$

By passing to the limit, we obtain $\limsup_{t \longrightarrow +\infty} x_{10}(t) = \limsup_{t \longrightarrow +\infty} \mathcal{B}(t) \leq \frac{(\alpha_1^{\varphi} + \alpha_2^{\varphi})\Lambda^{\varphi}}{\mu^{\varphi}\tau^{\varphi}}$.

Thus, Υ^{φ} is positively invariant and attracting for system (26).

References

[1] Hamadjam Abboubakar, Jean Claude Kamgang, and Daniel Tieudjo. Backward bifurcation and control in transmission dynamics of arboviral diseases. Mathematical biosciences, 278:100–129, 2016.

[2] Athifa Asma, Muhammad Altaf Khan, Kulpash Iskakova, Fuad S Al-Duais, and Irshad Ahmad. Mathematical modeling and analysis of the sars-cov-2 disease with reinfection. Computational Biology and Chemistry, page 107678, 2022.

[3] Adnane Boukhouima, Khalid Hattaf, El Mehdi Lotfi, Marouane Mahrouf, Delfim FM Torres, and Noura Yousfi. Lyapunov functions for fractional-order systems in biology: Methods and applications. Chaos, Solitons & Fractals, 140:110224, 2020.

[4] Tian-Mu Chen, Jia Rui, Qiu-Peng Wang, Ze-Yu Zhao, Jing-An Cui, and Ling Yin. A mathematical model for simulating the phase-based transmissibility of a novel coronavirus. Infectious Diseases of Poverty, 9(1):1–8, 2020.

[5] COVID-19 Tracker. Outil de suivi du COVID-19. https://bing.com/covid?vert=graph, Accessed 27-07-2022.

[6] B Cuahutenango-Barro, MA Taneco-Hernández, Yu-Pei Lv, JF Gómez-Aguilar, MS Osman, Hadi Jahanshahi, and Ayman A Aly. Analytical solutions of fractional wave equation with memory effect using the fractional derivative with exponential kernel. Results in Physics, 25:104148, 2021.

[7] Odo Diekmann, Johan Andre Peter Heesterbeek, and Johan AJ Metz. On the definition and the computation of the basic reproduction ratio r 0 in models for infectious diseases in heterogeneous populations. Journal of Mathematical Biology, 28(4):365–382, 1990.

[8] Kai Diethelm. A fractional calculus based model for the simulation of an outbreak of dengue fever. Nonlinear Dynamics, 71(4):613–619, 2013.

[9] Kai Diethelm, Neville J Ford, and Alan D Freed. A predictor-corrector approach for the numerical solution of fractional differential equations. Nonlinear Dynamics, 29(1-4):3–22, 2002.

[10] Kai Diethelm, Neville J Ford, and Alan D Freed. Detailed error analysis for a fractional Adams method. Numerical Algorithms, 36(1):31–52, 2004.

[11] Seraphin Djaoue, Gabriel Guilsou Kolaye, Hamadjam Abboubakar, Ado Adamou Abba Ari, and Irepran Damakoa. Mathematical modeling, analysis and numerical simulation of the COVID-19 transmission with mitigation of control strategies used in Cameroon. Chaos, Solitons & Fractals, 139:110281, 2020.

[12] Bogdan Doroftei, Alin Ciobica, Ovidiu-Dumitru Ilie, Radu Maftei, and Ciprian Ilea. Mini-review discussing the reliability and efficiency of covid-19 vaccines. Diagnostics, 11(4):579, 2021.

[13] Zhanwei Du, Lin Wang, Abhishek Pandey, Wey Wen Lim, Matteo Chinazzi, Eric HY Lau, Peng Wu, Anup Malani, Sarah Cobey, Benjamin J Cowling, et al. Modeling comparative cost-effectiveness of sars-cov-2 vaccine dose fractionation in india. Nature Medicine, 28(5):934–938, 2022.

[14] Firstpost. German covid-19 vaccine curevac has efficacy rate of 48 percent in final trials. https://www.firstpost.com/health/german-covid-19-vaccine-curevac-has-efficacy-rate-of-48-percent-in-final-trials-9769311.html, Accessed-June, 09 2022.

[15] Centers for Disease Control and Prevention (CDC). Science brief: Covid-19 vaccines and vaccination. https://www.cdc.gov/coronavirus/2019-ncov/science/science-briefs/fully-vaccinated-people.html, Accessed 20-04-2022.

[16] Brody H Foy, Brian Wahl, Kayur Mehta, Anita Shet, Gautam I Menon, and Carl Britto. Comparing COVID-19 vaccine allocation strategies in India: A mathematical modelling study. International Journal of Infectious Diseases, 103:431–438, 2021.

[17] Franceinfo. Campagne de vaccination contre le covid-19: en allemagne, un lent démarrage et déjá un premier couac. https://www.francetvinfo.fr/sante/maladie/coronavirus/vaccin/campagne-de-vaccination-contre-le-covid-19-en-allemagne-un-lent-demarrage-et-deja-un-premier-couac_4235369.html, 28/12/2020.

[18] Naleen Chaminda Ganegoda, Karunia Putra Wijaya, Miracle Amadi, KKW Erandi, and Dipo Aldila. Interrelationship between daily COVID-19 cases and average temperature as well as relative humidity in Germany. Scientific reports, 11(1):1–16, 2021.

[19] Salisu M Garba, Jean M-S Lubuma, and Berge Tsanou. Modeling the transmission dynamics of the COVID-19 Pandemic in South Africa. Mathematical Biosciences, 328:108441, 2020.

[20] Gauthier Sallet. Mathematical Epidemiology. https://iecl.univ-lorraine.fr/membre-iecl/sallet-gauthier/, March 2018.

[21] Nur 'Izzati Hamdan and Adem Kilicman. A fractional order SIR epidemic model for dengue transmission. Chaos, Solitons & Fractals, 114:55–62, 2018.

[22] Ritchie Hannah, Mathieu Edouard, Rodés-Guirao Lucas, Appel Cameron, Giattino Charlie, Ortiz-Ospina Esteban, Hasell Joe, Macdonald Bobbie, Dattani Saloni, and Roser Max. Coronavirus pandemic (covid-19). https://ourworldindata.org/coronavirus, Accessed March, 28 2022.

[23] Xingjie Hao, Shanshan Cheng, Degang Wu, Tangchun Wu, Xihong Lin, and Chaolong Wang. Reconstruction of the full transmission dynamics of COVID-19 in Wuhan. Nature, 584(7821):420–424, 2020.

[24] Rashid Jan, Muhammad Altaf Khan, Poom Kumam, and Phatiphat Thounthong. Modeling the transmission of dengue infection through fractional derivatives. Chaos, Solitons & Fractals, 127:189–216, 2019.

[25] Peter C Jentsch, Madhur Anand, and Chris T Bauch. Prioritising covid-19 vaccination in changing social and epidemiological landscapes: a mathematical modelling study. The Lancet Infectious Diseases, 21(8):1097–1106, 2021.

[26] Muhammad Altaf Khan and Abdon Atangana. Modeling the dynamics of novel coronavirus (2019-ncov) with fractional derivative. Alexandria Engineering Journal, 59(4):2379–2389, 2020.

[27] Pushpendra Kumar, Vedat Suat Erturk, Hamadjam Abboubakar, and Kottakkaran Sooppy Nisar. Prediction studies of the epidemic peak of coronavirus disease in Brazil via new generalised Caputo type fractional derivatives. Alexandria Engineering Journal, 60(3):3189–3204, 2021.

[28] Pushpendra Kumar, Norodin A Rangaig, Hamadjam Abboubakar, Anoop Kumar, and A Manickam. Prediction studies of the epidemic peak of coronavirus disease in japan: From caputo derivatives to atangana–baleanu derivatives. International Journal of Modeling, Simulation, and Scientific Computing, 13(01):2250012, 2022.

[29] Joseph P La Salle. The stability of dynamical systems. SIAM, 1976.

[30] Kaihui Liu and Yijun Lou. Optimizing covid-19 vaccination programs during vaccine shortages: A review of mathematical models. Infectious Disease Modelling, 2022.

[31] Peijiang Liu, Mati ur Rahman, and Anwarud Din. Fractal fractional based transmission dynamics of covid-19 epidemic model. Computer Methods in Biomechanics and Biomedical Engineering, pages 1–18, 2022.

[32] Zhihua Liu, Pierre Magal, Ousmane Seydi, and Glenn Webb. Understanding unreported cases in the COVID-19 epidemic outbreak in Wuhan, China, and the importance of major public health interventions. Biology, 9(3):50, 2020.

[33] Simeone Marino, Ian B Hogue, Christian J Ray, and Denise E Kirschner. A methodology for performing global uncertainty and sensitivity analysis in systems biology. Journal of theoretical biology, 254(1):178–196, 2008.

[34] Lemjini Masandawa, Silas Steven Mirau, and Isambi Sailon Mbalawata. Mathematical modeling of covid-19 transmission dynamics between healthcare workers and community. Results in Physics, 29:104731, 2021.

[35] SA Meo, IA Bukhari, J Akram, AS Meo, and DC Klonoff. Covid-19 vaccines: comparison of biological, pharmacological characteristics and adverse effects of pfizer/biontech and moderna vaccines. Eur. Rev. Med. Pharmacol Sci, 25(3):1663–1669, 2021.

[36] Gösta Magnus Mittag-Leffler. Sur la nouvelle fonction eα (x). CR Acad. Sci. Paris, 137(2):554–558, 1903.

[37] Sam Moore, Edward M Hill, Louise Dyson, Michael J Tildesley, and Matt J Keeling. Modelling optimal vaccination strategy for SARS-CoV-2 in the UK. PLoS Computational Biology, 17(5):e1008849, 2021.

[38] Sam Moore, Edward M Hill, Michael J Tildesley, Louise Dyson, and Matt J Keeling. Vaccination and non-pharmaceutical interventions for COVID-19: a mathematical modelling study. The Lancet Infectious Diseases, 21(6):793–802, 2021.

[39] Samuel Mwalili, Mark Kimathi, Viona Ojiambo, Duncan Gathungu, and Rachel Mbogo. SEIR model for COVID-19 dynamics incorporating the environment and social distancing. BMC Research Notes, 13(1):1–5, 2020.

[40] Khondoker Nazmoon Nabi, Hamadjam Abboubakar, and Pushpendra Kumar. Forecasting of covid-19 pandemic: From integer derivatives to fractional derivatives. Chaos, Solitons & Fractals, 141:110283, 2020.

[41] Parvaiz Ahmad Naik, Kolade M Owolabi, Jian Zu, and Mehraj-Ud-Din Naik. Modeling the transmission dynamics of covid-19 pandemic in caputo type fractional derivative. Journal of Multiscale Modelling, 12(03):2150006, 2021.

[42] Faïçal Ndaïrou, Iván Area, Juan J Nieto, and Delfim FM Torres. Mathematical modeling of COVID-19 transmission dynamics with a case study of Wuhan. Chaos, Solitons & Fractals, 135:109846, 2020.

[43] Calistus N Ngonghala, Enahoro Iboi, Steffen Eikenberry, Matthew Scotch, Chandini Raina MacIntyre, Matthew H Bonds, and Abba B Gumel. Mathematical assessment of the impact of non-pharmaceutical interventions on curtailing the 2019 novel coronavirus. Mathematical Biosciences, 325:108364, 2020.

[44] A Omame, D Okuonghae, Ugochukwu K Nwajeri, and Chibueze P Onyenegecha. A fractional-order multi-vaccination model for covid-19 with non-singular kernel. Alexandria Engineering Journal, 61(8):6089–6104, 2022.

[45] Igor Podlubny. Fractional differential equations: an introduction to fractional derivatives, fractional differential equations, to methods of their solution and some of their applications. Elsevier, 1998.

[46] Ronald Ross. Some quantitative studies in epidemiology. Nature, 87(2188):466–467, 1911.

[47] Nuru Saadi, Y Chi, Srobana Ghosh, Rosalind M Eggo, Ciara V McCarthy, Matthew Quaife, Jeanette Dawa, Mark Jit, Anna Vassall, et al. Models of covid-19 vaccine prioritisation: a systematic literature search and narrative review. BMC Medicine, 19(1):1–11, 2021.

[48] Amer M Salman, Issam Ahmed, Mohd Hafiz Mohd, Mohammad Subhi Jamiluddin, and Mohammed Ali Dheyab. Scenario analysis of covid-19 transmission dynamics in malaysia with the possibility of reinfection and limited medical resources scenarios. Computers in biology and medicine, 133:104372, 2021.

[49] Zhong-Hua Shen, Yu-Ming Chu, Muhammad Altaf Khan, Shabbir Muhammad, Omar A Al-Hartomy, and M Higazy. Mathematical modeling and optimal control of the covid-19 dynamics. Results in Physics, 31:105028, 2021.

[50] Muhammad Sher, Kamal Shah, Zareen A Khan, Hasib Khan, and Aziz Khan. Computational and theoretical modeling of the transmission dynamics of novel COVID-19 under Mittag-Leffler power law. Alexandria Engineering Journal, 59(5):3133–3147, 2020.

[51] Zhisheng Shuai and Pauline van den Driessche. Global stability of infectious disease models using Lyapunov functions. SIAM Journal on Applied Mathematics, 73(4):1513–1532, 2013.

[52] Mircea T Sofonea, Bastien Reyné, Baptiste Elie, Ramsès Djidjou-Demasse, Christian Selinger, Yannis Michalakis, and Samuel Alizon. Memory is key in capturing COVID-19 epidemiological dynamics. Epidemics, 35:100459, 2021.

[53] Michael Stein. Large sample properties of simulations using latin hypercube sampling. Technometrics, 29(2):143–151, 1987.

[54] Nicholas Steyn, Michael J Plank, Rachelle N Binny, Shaun C Hendy, Audrey Lustig, and Kannan Ridings. A covid-19 vaccination model for aotearoa new zealand. Scientific Reports, 12(1):1–11, 2022.

[55] Calvin Tadmon and Severin Foko. A transmission dynamics model of Covid-19: Case of Cameroon. Infectious Disease Modelling, 2022.

[56] Sabri TM Thabet, Mohammed S Abdo, Kamal Shah, and Thabet Abdeljawad. Study of transmission dynamics of covid-19 mathematical model under abc fractional order derivative. Results in Physics, 19:103507, 2020.

[57] Pauline Van den Driessche and James Watmough. Reproduction numbers and sub-threshold endemic equilibria for compartmental models of disease transmission. Mathematical Biosciences, 180(1-2):29–48, 2002.

[58] Jin-Liang Wang and Hui-Feng Li. Surpassing the fractional derivative: Concept of the memory-dependent derivative. Computers & Mathematics with Applications, 62(3):1562–1567, 2011.

[59] Oliver J Watson, Gregory Barnsley, Jaspreet Toor, Alexandra B Hogan, Peter Winskill, and Azra C Ghani. Global impact of the first year of covid-19 vaccination: a mathematical modelling study. The Lancet Infectious Diseases, 2022.

[60] World Health Organization. Covid-19 vaccines. https://www.paho.org/fr/vaccins-anti-covid-19, 2021.

[61] World Health Organization and others. Coronavirus disease 2019 (covid-19): situation report, 82. World Health Organization, 2020.

[62] World Health Organization (WHO. Status of Covid-19 Vaccines within WHO EUL/PQ evaluation process. https://en.wikipedia.org/wiki/List_of_COVID-19_vaccine_authorizations, Accessed 27-07-2022.

[63] Jianyong Wu, Radhika Dhingra, Manoj Gambhir, and Justin V Remais. Sensitivity analysis of infectious disease models: methods, advances and their application. Journal of The Royal Society Interface, 10(86):20121018, 2013.

[64] Dazhi Zhao and Maokang Luo. Representations of acting processes and memory effects: general fractional derivative and its application to theory of heat conduction with finite wave speeds. Applied Mathematics and Computation, 346:531–544, 2019.

[65] Linhua Zhou and Meng Fan. Dynamics of an sir epidemic model with limited medical resources revisited. Nonlinear Analysis: Real World Applications, 13(1):312–324, 2012.